OTTER: Effortless Label Distribution Adaptation of Zero-shot Models

Changho Shin [1] **Jitian Zhao** [1] **Sonia Cromp** [1] **Harit Vishwakarma** [1] **Frederic Sala** [1]

Abstract

Popular zero-shot models suffer due to artifacts inherited from pretraining. One particularly detrimental issue, caused by unbalanced web-scale pretraining data, is *mismatched label distribution*. Existing approaches that seek to repair the label distribution are not suitable in zero-shot settings, as they have mismatching requirements, such as needing access to labeled downstream task data or knowledge of the true label balance in the pretraining distribution. We sidestep these challenges and introduce a simple and lightweight approach to adjust pretrained model predictions via optimal transport. Our technique requires only an *estimate* of the label distribution of a downstream task. Theoretically, we characterize the improvement produced by our procedure under certain mild conditions and provide bounds on the error caused by misspecification. Empirically, we validate our method in a wide array of zero-shot image and text classification tasks, improving accuracy by 4.8% and 15.9% on average, and beating baselines like prior matching—often by significant margins—in 17 out of 21 datasets.

1. Introduction

Zero-shot models are popular but struggle with biases inherited from their large pretraining datasets (Dixon et al., 2018; Torralba & Efros, 2011; Agarwal et al., 2021). In particular, zero-shot classification is strongly biased by *the label distribution* of the pretraining task. When the label distribution of the downstream task differs from pretraining, the performance of zero-shot classifiers suffers greatly. For example, Figure 1 illustrates the effects of mismatched distributions on a pet image classification task. Two CLIP models (RN50, and ViT-B/16) produce biased predictions on the `Abyssinian` and `Persian` classes. Furthermore,

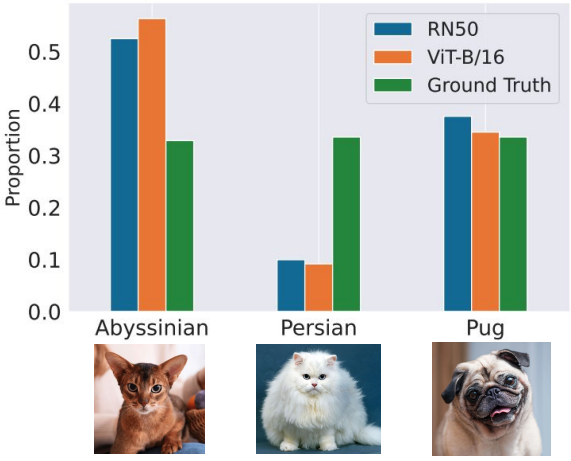

Figure 1. Label distribution mismatch example in zero-shot classification. In Oxford-IIIT-Pet dataset, the labels are uniformly distributed, while the zero-shot models exhibit biased predictions toward some clasess. This bias is influenced by the distribution of labels in the pretraining task.

datasets with a large number of classes, such as ImageNet, may contain both extremely common and very rare classes, resulting in an outsized probability that a zero-shot model will predict some classes over others. As a result, even large models intended for use in zero-shot settings, such as CLIP (Radford et al., 2021), naturally have a label distribution mismatch between pretraining data and downstream tasks.

Existing methods that seek to address label distribution *make strong assumptions or have expensive requirements*. For example, to fine-tune a model, we must obtain a labeled fine-tuning dataset of adequate size, then obtain the time and compute to further train the model. To perform label shift adaptation techniques, we must know the true label distribution of the pretraining distribution—difficult to impossible for real-world tasks.

Can we deal with label distribution mismatch ***without additional training or access to ground-truth downstream task information***? While seemingly challenging, one cause for optimism is the observation that zero-shot models still give relatively high prediction probabilities for correct classes, though classes common in pretraining tend to have relatively inflated scores overall. Intuitively, the model has already

[1]Department of Computer Sciences, University of Wisconsin–Madison, United States. Correspondence to: Changho Shin <cshin23@wisc.edu>.

Proceedings of the 41st International Conference on Machine Learning, Vienna, Austria. PMLR 235, 2024. Copyright 2024 by the author(s).

learned to identify examples of its downstream classes (and so does not require further training) and is already impacted by the pretraining label distribution (and so does not need access to the ground-truth pretraining label distribution). Instead, the model's prediction probabilities must be adjusted based on an estimated downstream label distribution specification.

To perform this label distribution adjustment, we view zero-shot learning through the lens of optimal transport (OT) and develop a technique called **OTTER (Optimal TransporT adaptER)**. This OT-based approach offers a systematic way to rebalance predicted labels: data points are transported to optimal downstream classes, minimizing the overall cost in accordance with the estimated the downstream label distribution specifications.

Theoretically, we show that optimal transport given the true label distribution of the downstream can recover the Bayes-optimal classifier under mild conditions. Additionally, we provide error bounds on our adaptation method for misspecification. We provide synthetic experiments validating our theoretical claims. In real-world data settings, we validate our method on a wide variety of image and text classification tasks, showing 4.8% and 15.5% accuracy improvement on average in image and text zero-shot classification tasks, respectively.

- OTTER, an algorithm to deal with label distribution mismatch at inference time via optimal transport,
- Theoretical results showing the effectiveness of our method, including the ability to recover the Bayes-optimal classifier and a sensitivity analysis with respect to the label distribution specification estimation,
- Extensive empirical results on zero-shot classification for text and image datasets, showing accuracy improvements of up to 25% and
- Experimental results demonstrating the applicability of OTTER to few-shot settings, showing accuracy improvements of up to 15%, even with noisy label distribution specification. (Appendix E.5)

2. Problem Formulation

Let $X = \{x_1, x_2, \ldots, x_n\}$ be an inference dataset with $x_i \in \mathcal{X}$. Furthermore, let $Y = \{y_1, y_2, \ldots, y_n\}$ be the true labels of the K-class classification dataset, such that $y_i \in \mathcal{Y} = [K]$, are sampled according to the downstream label distribution $\nu = (p_1, p_2, \ldots, p_K)$.

Let $s_\theta(x, j) := P_\theta(Y = j|X = x)$ be a pretrained classification model constrained to the downstream label space. During pretraining, s_θ has been biased to the source label distribution ν^s. We wish to offset such label distribution bias with a label distribution specification $\hat{\nu}$ for the target distribution. $\hat{\nu}$ is expected to be closer to the true label distribution of the downstream task. Given a label distribution specification, our goal is to rebalance predictions so that the predicted label distribution follows the label distribution specification.

Algorithm 1 OTTER

1: **Input:** Input $\mathbf{X} = \{x_1, \ldots, x_n\}$, label distribution specification $(p_1, \ldots, p_K)$, cost matrix $C \in \mathbb{R}^{n \times K}$
2: Define input marginal $\mu = \mathbf{1}\frac{1}{n}$, prediction marginal $\nu = (p_1, \ldots, p_K)$
3: Run optimal transport and obtain transport plan π s.t. $\pi = \arg\min_{\gamma \in \Pi(\mu,\nu)} \langle \gamma, C \rangle$.
4: Get modified classification outputs $\hat{y}_i = \arg\max_{j \in [K]} \pi_{i,j}$.
Return $\{\hat{y}_i\}_{i \in [n]}$

3. Proposed Framework

We propose OTTER (Optimal TransporT adaptER), an optimal transport-based label distribution adaptation approach. Our goal is to have the n input data points allocated to K classes match a given label distribution $\hat{\nu}$, where $\sum_{j=1}^{K} \hat{\nu}_j = 1, \hat{\nu}_j \geq 0$. Specifically, we want to classify $n\hat{\nu}_1$ points as the first class, $n\hat{\nu}_2$ points as the second, and so on. However, there are many such allocations, and it is not a priori clear which one should be selected. We propose formulating an optimal transport problem that selects the allocation minimizing a particular cost:

$$\pi = \arg\min_{\gamma \in \Pi(\mu, \hat{\nu})} \langle \gamma, C \rangle,$$

where $\Pi(\mu, \hat{\nu}) = \{\gamma \in \mathbb{R}_+^{n \times K} | \gamma \mathbf{1} = \mu, \gamma^T \mathbf{1} = \hat{\nu}\}, \mu = \frac{1}{n}\mathbf{1}$ and C is the cost (loss) matrix such that C_{ij} represents a loss when we classify x_i as class j. This procedure is described in Algorithm 1. Note that this procedure naturally matches the given label distribution specification $\hat{\nu}$.

We wish to use Algorithm 1 for zero-shot classification given the pretrained model s_θ. To do so, we must select a cost function and produce C_{ij}. An ideal choice of such a function is $C_{ij} = -\log_t P_t(Y = j|X = i)$ such that optimal transport minimizes the negative log posterior under constraints. However, the target distribution P_t is unknown. Instead, we replace the posterior with the classifier scores $s_\theta(x_i, j)$. We highlight that this choice of cost matrix is an natural extension of zero-shot classification under the label distribution constraint. We prove this claim in the next section.

4. Theoretical Results

In practical scenarios, label distribution specifications are frequently subject to noise, and prediction probabilities may

not be well-calibrated. To understand the impact of these factors, we examine how errors in label distribution specification and calibration influence the transport plan. Our theoretical analysis yields following findings: (a) classification can be interpreted as an optimal transport, (b) OTTER can recover the Bayes-optimal classifier in the label shift setting, (c) for a noisy cost matrix with the noisy label distribution specification setup, the suboptimality can be bounded by the deviation of cost matrix and label distribution. We state our main theorems. See Appendix D for the details.

Theorem 4.1 (Classification as optimal transport)**.** *Let* $\nu_j^{ZS} = \frac{1}{n}\sum_{i=1}^{n} \mathbb{1}[\hat{y}_i^{ZS} = j]$, *where* $\hat{y}_i^{ZS} = \arg\max_{j' \in [K]} P_\theta(Y = j'|X = x_i)$. *Then, given* $C_{ij} = -\log P_\theta(Y = j|X = x_i), \pi = \arg\min_{\gamma \in \Pi(\mu, \nu^{ZS})} \langle \gamma, C \rangle, \hat{y}_i^{OT} = \arg\max_{j \in [K]} \pi_{ij}$. *Assuming there are no ties in scores, i.e.* $P_\theta(Y = j|X = x_i) \neq P_\theta(Y = j'|X = x_i)$, *for all* $j \neq j'$, *the predictions are equivalent, i.e.* $\hat{y}_i^{OT} = \hat{y}_i^{ZS}$ *for all* $i \in [n]$.

Theorem 4.2 (Label shift invariance)**.** *Suppose the pretrained model is well-calibrated for the source distribution,*

$$P_\theta(Y = j|X = x_i) = P_s(Y = j|X = x_i)$$

and there is no tie probability, for all $j \neq j', i \in [n]$

$$P_\theta(Y = j|X = x_i) \neq P_\theta(Y = j'|X = x_i).$$

Denote the Bayes optimal predictions in the target distribution as $\hat{y}_i^* = \arg\max_{j \in [K]} \log P_t(Y = j|X = x_i)$. *Then* OTTER *predictions* $\text{OTTER}(\mathbf{X}, P_t(Y), C)$ *are the same as Bayes optimal predictions* $\hat{y}^*$.

Corollary 4.1 (Suboptimality bound)**.** *Let the primal linear programming problem be defined as in equation (1), and its dual problem be* $max\{w^T g | w^T G \leq vec(C)^T, w \geq 0\}$. *Suppose perturbed cost matrix is* $\hat{C} = C + \Delta_C$, *the perturbed class distribution* $\hat{\nu} = \nu + \Delta_\nu$, *such that* $\hat{g} = g + \Delta_g$ *where*

$$\Delta_g = \begin{bmatrix} 0 \\ \hat{\nu} - \nu \\ 0 \\ -\hat{\nu} + \nu \end{bmatrix}.$$

Assume that primal and dual problems are solvable. Denote the original solutions as π, w *and perturbed solutions as* $\hat{\pi}$ *and* $\hat{w}$. *Define the classification rule determined by transportation plan as* f_π *and* $f_{\hat{\pi}}$. *The prediction accuracy of the perturbed transport plan can be lower bounded as:*

$$Acc(f_{\hat{\pi}}) = \sum_{i=1}^{n} \mathbf{1}[f_\pi(x_i) = f_{\hat{\pi}}(x_i)]/n \geq 1 - \frac{n\epsilon_n^2}{2},$$

where $\epsilon_n = \kappa(\|\Delta_\nu\|_2 + \|[vec(\Delta_C)]_+\|_2 + \|vec(C)^T vec(\hat{\pi}) - g^T \hat{w}\|_2)$.

5. Experiments

The primary objective of our experiments is to (1) validate that OTTER improves zero-shot model performance when given accurate label distribution estimates and (2) investigate its sensitivity to perturbations. In experiments on real datasets (Section 5.1), we confirm that OTTER can improve zero-shot classification significantly in a variety of settings. In synthetic experiments (Section 5.2), we validate our theoretical claims—label shift invariance and sensitivity to perturbation in a fully controllable setting. Additionally, we show that OTTER can be combined with label distribution estimation methods in the few-shot learning setting (Section E.4). Finally, we show that OTTER especially benefits hierarchical classification (Section E.6).

5.1. Real Data Experiments

We hypothesize that the model performance can improve significantly when the label distribution specification is exact.

Setup and Procedure. We used 17 image classification datasets and 4 text classification datasets. We employed CLIP (Radford et al., 2021) for image zero-shot classification, and BERT (Devlin et al., 2018). A comprehensive list and details of experiments can be found in Appendix E.

Baseline. We adopt Prior Matching (PM) (Liusie et al., 2023) as a baseline. It optimizes score weighting parameters to align with the label distribution specification. A detailed explanation of Prior Matching is given in Appendix C. It is worth noting that the performance of *Prior Matching is highly sensitive to hyperparameters such as temperature and learning rate*. Optimal hyperparameters may vary across different datasets. We selected hyperparameters through grid search, by evaluating their performance on a validation set, consisting of 10 labeled examples per class. In contrast, we highlight that OTTER is tuning-free.

Results. Table 1 shows the image classification results with CLIP (ViT-B/16) and the text classification results with BERT. Notably, OTTER *demonstrates a 4.8% and 15.5% enhancement on average in image and text zero-shot classification, respectively*. While Prior Matching shows competitive performance when accurately tuned, it often struggles. We found that hyperparameter tuning fails in the class-imbalanced datasets such as Caltech256, SUN397, ImageNet-r (Appendix E, Table 3). This suggests that the hyperparameter selection process necessitates a validation set label distribution similar to the target distribution—rendering it unusable in zero-shot scenarios. More details and additional experiment results — including the sensitivity study on the label distribution specification error, computation time, and combination with other prompting methods — are provided in Appendix E.3.

	Zero-shot	Prior Matching	OTTER		Zero-shot	Prior Matching	OTTER
CIFAR10	88.3	91.3 (±0.0)	**91.7**	Oxford-IIIT-Pet	83.8	82.0 (±0.3)	**88.8**
CIFAR100	63.8	64.1 (±2.7)	**67.9**	Stanford-Cars	55.7	39.8 (±2.6)	**59.7**
Caltech101	79.8	59.3 (±15.4)	**88.7**	STL10	98.0	98.4 (±0.0)	**98.6**
Caltech256	79.8	9.5 (±1.5)	**87.0**	SUN397	47.1	6.7 (±1.6)	**54.1**
Country211	19.8	19.0 (±0.1)	**21.1**	CUB	46.0	40.4 (±0.0)	**50.4**
DTD	39.0	42.1 (±0.1)	**44.4**	ImageNet	60.2	53.6 (±0.1)	**62.9**
EUROSAT	32.9	41.6 (±0.8)	**42.0**	ImageNet-r	68.9	16.7 (±3.5)	**72.4**
Flowers102	64.0	54.0 (±14.1)	**70.8**	ImageNet-Sketch	39.8	36.5 (±0.4)	**44.5**
Food101	85.6	86.8 (±3.1)	**89.9**				
Amazon review	74.0	58.8 (±46.4)	**91.7**	GenderBias	84.1	41.4 (±39.6)	**91.9**
CivilComments	48.4	57.2 (±37.7)	**81.4**	HateXplain	30.9	31.3 (±3.3)	**34.3**

Table 1. Accuracy (%) in zero-shot image classification (ViT-B/16) and text classification (BERT). We use the true label distribution as the label distribution specification. The numbers in parenthesis of Prior Matching represent the standard deviation of 10 different samplings of the validation set. OTTER produces improvements nearly across-the-board, with an average lift 4.9% in image classification and 15.5% in text classification, outperforming a powerful baseline, prior matching in almost all cases.

5.2. Synthetic Experiments

We hypothesize OTTER is invariant to label shift under the conditions in Theorem 4.2. We also investigate the sensitivity to perturbations of the cost matrix and the label distribution.

Setup and Procedure. We simulate label shift in logistic regression on gaussian mixtures. We compare a naive logistic regression model, OTTER, and a bayes classifier. We separately investigate perturbed prediction score matrix and perturbed label distribution's impact on the prediction accuracy. For perturbed prediction scores, we fix the label distribution to be the true one, and add noise $\delta \sim \mathcal{N}(0, \sigma^2)$ of varying levels σ to the predicted score $P_\theta(Y = 1|X)$. For label distribution, we fix the prediction score to be true scores and add noise ϵ: $\hat{\nu} = \nu^t + (\epsilon, -\epsilon)$. We use these perturbed variants to obtain perturbed solutions and compare with ground-truth solution. For the details of synthetic dataset and classifiers, refer Appendix E.

Results. Figure 2 illustrates how accuracy changes with label shift when the predicted score is perturbed and when label distribution is perturbed. We observe that the naive classifier deteriorates as the total variation distance between source and target distributions increases. It indicates that naive classifier is sensitive to label shift. However, without perturbation, OTTER *remains unaffected by the label distribution shift*, which validates our invariance result in Section 4.

In the case of confidence score perturbation, both the naive classifier and OTTER have accuracy decreasing as perturbation level increases. For simplicity, we omitted the naive classifier's performances under different levels of noise as adding zero-mean noise does not alter its accuracy significantly. We observe that OTTER has better performance than the naive method when significant label shift exists. Similarly, for label distribution perturbation, we observe as the noise level ϵ increases, OTTER's accuracy downgrades—but still yields better performance when label shift is severe.

Our experimental results suggest simply applying predicted score for zero-shot classification leads to inaccurate predictions under label shift, while OTTER is robust to label shift when no perturbation existed. Perturbations in both predicted score and label distribution downgrades the predicted accuracy, as expected, but OTTER still yields better results than the naive baseline.

6. Conclusion

While zero-shot models have been successful, pretraining using Internet-scale datasets yields artifacts that may harm downstream tasks. In this paper, we identify the bias in class balance, and provide a simple but powerful solution using optimal transport. Theoretically, we describe how OT can fix label distribution mismatch and its sensitivity to perturbations. Empirically, we validated our approach's ability to improve zero-shot classification accuracy, mitigating label distribution mismatch in zero-shot models. We believe our method can expedite the deployment of zero-shot classification, reducing the necessity of finetuning for downstream tasks.

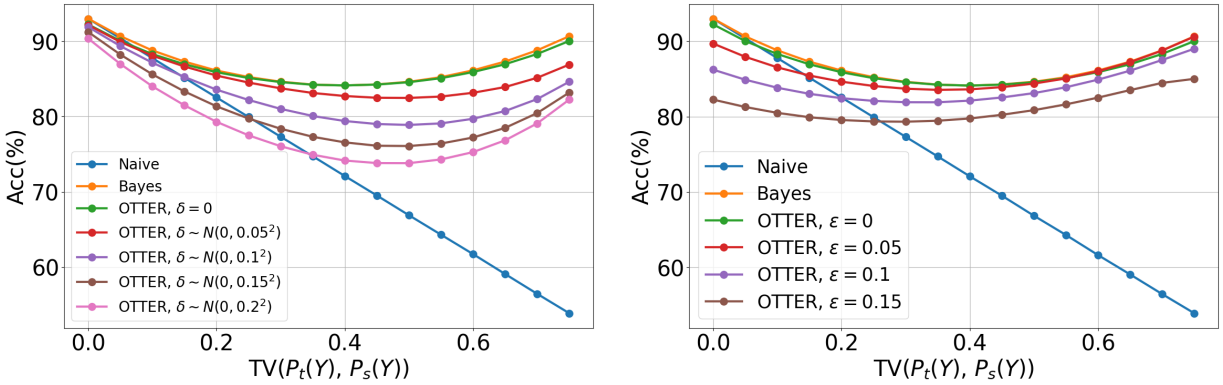

(a) Prediction accuracy changes with perturbed confidence score.

(b) Prediction accuracy changes with perturbed label distribution.

Figure 2. Synthetic experiment results. X-axis represents total variation distance between the source and the target distribution, describing label shift severity. Y-axis represents prediction accuracy. Curves represent different methods and noise levels. Our approaches dramatically outperform the baseline at higher mismatch levels.

Impact statement This paper presents work whose goal is to advance the field of Machine Learning. There are many potential societal consequences of our work, none which we feel must be specifically highlighted here. As of now, we are not aware of additional potential societal impacts beyond the typical implications associated with zero-shot models.

References

Adila, D., Shin, C., Cai, L., and Sala, F. Zero-shot robustification of zero-shot models. In *The Twelfth International Conference on Learning Representations*, 2023.

Agarwal, S., Krueger, G., Clark, J., Radford, A., Kim, J. W., and Brundage, M. Evaluating clip: towards characterization of broader capabilities and downstream implications. *arXiv preprint arXiv:2108.02818*, 2021.

Alexandari, A., Kundaje, A., and Shrikumar, A. Maximum likelihood with bias-corrected calibration is hard-to-beat at label shift adaptation. In *International Conference on Machine Learning*, pp. 222–232. PMLR, 2020.

An, B., Zhu, S., Panaitescu-Liess, M.-A., Mummadi, C. K., and Huang, F. More context, less distraction: Visual classification by inferring and conditioning on contextual attributes. *arXiv preprint arXiv:2308.01313*, 2023.

Azé, D. and Corvellec, J.-N. On the sensitivity analysis of hoffman constants for systems of linear inequalities. *SIAM Journal on Optimization*, 12(4):913–927, 2002.

Azizzadenesheli, K., Liu, A., Yang, F., and Anandkumar, A. Regularized learning for domain adaptation under label shifts. In *International Conference on Learning Representations*, 2019.

Borkan, D., Dixon, L., Sorensen, J., Thain, N., and Vasserman, L. Nuanced metrics for measuring unintended bias with real data for text classification. In *Companion proceedings of the 2019 world wide web conference*, pp. 491–500, 2019.

Bossard, L., Guillaumin, M., and Van Gool, L. Food-101–mining discriminative components with random forests. In *Computer Vision–ECCV 2014: 13th European Conference, Zurich, Switzerland, September 6-12, 2014, Proceedings, Part VI 13*, pp. 446–461. Springer, 2014.

Chang, W., Shi, Y., Tuan, H., and Wang, J. Unified optimal transport framework for universal domain adaptation. *Advances in Neural Information Processing Systems*, 35: 29512–29524, 2022.

Chawla, N. V., Bowyer, K. W., Hall, L. O., and Kegelmeyer, W. P. Smote: synthetic minority over-sampling technique. *Journal of artificial intelligence research*, 16:321–357, 2002.

Chuang, C.-Y., Jampani, V., Li, Y., Torralba, A., and Jegelka, S. Debiasing vision-language models via biased prompts. *arXiv preprint arXiv:2302.00070*, 2023.

Cimpoi, M., Maji, S., Kokkinos, I., Mohamed, S., and Vedaldi, A. Describing textures in the wild. In *Proceedings of the IEEE conference on computer vision and pattern recognition*, pp. 3606–3613, 2014.

Coates, A., Ng, A., and Lee, H. An analysis of single-layer networks in unsupervised feature learning. In *Proceedings of the fourteenth international conference on artificial intelligence and statistics*, pp. 215–223. JMLR Workshop and Conference Proceedings, 2011.

Deng, J., Dong, W., Socher, R., Li, L.-J., Li, K., and Fei-Fei, L. Imagenet: A large-scale hierarchical image database. In *2009 IEEE conference on computer vision and pattern recognition*, pp. 248–255. Ieee, 2009.

Devlin, J., Chang, M.-W., Lee, K., and Toutanova, K. Bert: Pre-training of deep bidirectional transformers for language understanding. *arXiv preprint arXiv:1810.04805*, 2018.

Dinan, E., Fan, A., Wu, L., Weston, J., Kiela, D., and Williams, A. Multi-dimensional gender bias classification. In *Proceedings of the 2020 Conference on Empirical Methods in Natural Language Processing (EMNLP)*, pp. 314–331, Online, November 2020. Association for Computational Linguistics. doi: 10.18653/v1/2020.emnlp-main.23. URL https://www.aclweb.org/anthology/2020.emnlp-main.23.

Dixon, L., Li, J., Sorensen, J., Thain, N., and Vasserman, L. Measuring and mitigating unintended bias in text classification. 2018.

Fei-Fei, L., Fergus, R., and Perona, P. One-shot learning of object categories. *IEEE transactions on pattern analysis and machine intelligence*, 28(4):594–611, 2006.

Fernández, A., García, S., Galar, M., Prati, R. C., Krawczyk, B., and Herrera, F. *Learning from imbalanced data sets*, volume 10. Springer, 2018.

Garg, S., Wu, Y., Balakrishnan, S., and Lipton, Z. A unified view of label shift estimation. *Advances in Neural Information Processing Systems*, 33:3290–3300, 2020.

Griffin, G., Holub, A., and Perona, P. Caltech-256 object category dataset. 2007.

Guo, D., Li, Z., Zhao, H., Zhou, M., Zha, H., et al. Learning to re-weight examples with optimal transport for imbalanced classification. *Advances in Neural Information Processing Systems*, 35:25517–25530, 2022.

Helber, P., Bischke, B., Dengel, A., and Borth, D. Eurosat: A novel dataset and deep learning benchmark for land use and land cover classification. *IEEE Journal of Selected Topics in Applied Earth Observations and Remote Sensing*, 12(7):2217–2226, 2019.

Hendrycks, D., Basart, S., Mu, N., Kadavath, S., Wang, F., Dorundo, E., Desai, R., Zhu, T., Parajuli, S., Guo, M., et al. The many faces of robustness: A critical analysis of out-of-distribution generalization. In *Proceedings of the IEEE/CVF International Conference on Computer Vision*, pp. 8340–8349, 2021.

Hoffman, A. J. On approximate solutions of systems of linear inequalities. *Journal of Research of the National Bureau of Standards*, 49(4), 1952.

Kahana, J., Cohen, N., and Hoshen, Y. Improving zero-shot models with label distribution priors. *arXiv preprint arXiv:2212.00784*, 2022.

Krause, J., Stark, M., Deng, J., and Fei-Fei, L. 3d object representations for fine-grained categorization. In *Proceedings of the IEEE international conference on computer vision workshops*, pp. 554–561, 2013.

Krizhevsky, A., Hinton, G., et al. Learning multiple layers of features from tiny images. 2009.

Lipton, Z., Wang, Y.-X., and Smola, A. Detecting and correcting for label shift with black box predictors. In *International conference on machine learning*, pp. 3122–3130. PMLR, 2018a.

Lipton, Z., Wang, Y.-X., and Smola, A. Detecting and correcting for label shift with black box predictors. In *International conference on machine learning*, pp. 3122–3130. PMLR, 2018b.

Liu, H., Li, C., Wu, Q., and Lee, Y. J. Visual instruction tuning. *arXiv preprint arXiv:2304.08485*, 2023.

Liusie, A., Manakul, P., and Gales, M. J. Mitigating word bias in zero-shot prompt-based classifiers. *arXiv preprint arXiv:2309.04992*, 2023.

Loshchilov, I. and Hutter, F. Decoupled weight decay regularization. In *International Conference on Learning Representations*, 2018.

Mathew, B., Saha, P., Yimam, S. M., Biemann, C., Goyal, P., and Mukherjee, A. Hatexplain: A benchmark dataset for explainable hate speech detection. In *Proceedings of the AAAI Conference on Artificial Intelligence*, volume 35, pp. 14867–14875, 2021.

Menon, S. and Vondrick, C. Visual classification via description from large language models. *arXiv preprint arXiv:2210.07183*, 2022.

Ni, J., Li, J., and McAuley, J. Justifying recommendations using distantly-labeled reviews and fine-grained aspects. In *Proceedings of the 2019 conference on empirical methods in natural language processing and the 9th international joint conference on natural language processing (EMNLP-IJCNLP)*, pp. 188–197, 2019.

Nilsback, M.-E. and Zisserman, A. Automated flower classification over a large number of classes. In *2008 Sixth Indian conference on computer vision, graphics & image processing*, pp. 722–729. IEEE, 2008.

Novack, Z., McAuley, J., Lipton, Z. C., and Garg, S. Chils: Zero-shot image classification with hierarchical label sets. In *International Conference on Machine Learning*, pp. 26342–26362. PMLR, 2023.

Parkhi, O. M., Vedaldi, A., Zisserman, A., and Jawahar, C. Cats and dogs. In *2012 IEEE conference on computer vision and pattern recognition*, pp. 3498–3505. IEEE, 2012.

Pena, J., Vera, J. C., and Zuluaga, L. F. New characterizations of hoffman constants for systems of linear constraints. *Mathematical Programming*, 187:79–109, 2021.

Peña, J. F. An easily computable upper bound on the hoffman constant for homogeneous inequality systems. *Computational Optimization and Applications*, 87(1):323–335, 2024.

Peng, H., Sun, M., and Li, P. Optimal transport for long-tailed recognition with learnable cost matrix. In *International Conference on Learning Representations*, 2021.

Peyré, G., Cuturi, M., et al. Computational optimal transport: With applications to data science. *Foundations and Trends® in Machine Learning*, 11(5-6):355–607, 2019.

Radford, A., Kim, J. W., Hallacy, C., Ramesh, A., Goh, G., Agarwal, S., Sastry, G., Askell, A., Mishkin, P., Clark, J., et al. Learning transferable visual models from natural language supervision. In *International conference on machine learning*, pp. 8748–8763. PMLR, 2021.

Reimers, N. and Gurevych, I. Sentence-bert: Sentence embeddings using siamese bert-networks. *arXiv preprint arXiv:1908.10084*, 2019.

Roberts, N., Li, X., Adila, D., Cromp, S., Huang, T.-H., Zhao, J., and Sala, F. Geometry-aware adaptation for pre-trained models. In *Thirty-seventh Conference on Neural Information Processing Systems*, 2023.

Robinson, S. M. Bounds for error in the solution set of a perturbed linear program. *Linear Algebra and its applications*, 6:69–81, 1973.

Santambrogio, F. Optimal transport for applied mathematicians. *Birkäuser, NY*, 55(58-63):94, 2015.

Shi, L., Zhen, H., Zhang, G., and Yan, J. Relative entropic optimal transport: a (prior-aware) matching perspective to (unbalanced) classification. *Advances in Neural Information Processing Systems*, 36, 2024.

Tachet des Combes, R., Zhao, H., Wang, Y.-X., and Gordon, G. J. Domain adaptation with conditional distribution matching and generalized label shift. *Advances in Neural Information Processing Systems*, 33:19276–19289, 2020.

Tai, K. S., Bailis, P. D., and Valiant, G. Sinkhorn label allocation: Semi-supervised classification via annealed self-training. In *International Conference on Machine Learning*, pp. 10065–10075. PMLR, 2021.

Thai-Nghe, N., Gantner, Z., and Schmidt-Thieme, L. Cost-sensitive learning methods for imbalanced data. In *The 2010 International joint conference on neural networks (IJCNN)*, pp. 1–8. IEEE, 2010.

Torralba, A. and Efros, A. A. Unbiased look at dataset bias. In *CVPR 2011*, pp. 1521–1528, 2011. doi: 10.1109/CVPR.2011.5995347.

Wah, C., Branson, S., Welinder, P., Perona, P., and Belongie, S. The caltech-ucsd birds-200-2011 dataset. 2011.

Wang, H., Ge, S., Lipton, Z., and Xing, E. P. Learning robust global representations by penalizing local predictive power. *Advances in Neural Information Processing Systems*, 32, 2019.

Wang, H., Xia, M., Li, Y., Mao, Y., Feng, L., Chen, G., and Zhao, J. Solar: Sinkhorn label refinery for imbalanced partial-label learning. *Advances in Neural Information Processing Systems*, 35:8104–8117, 2022.

Wei, J., Bosma, M., Zhao, V. Y., Guu, K., Yu, A. W., Lester, B., Du, N., Dai, A. M., and Le, Q. V. Finetuned language models are zero-shot learners. *arXiv preprint arXiv:2109.01652*, 2021.

Xian, R., Yin, L., and Zhao, H. Fair and optimal classification via post-processing. 2023.

Xiao, J., Hays, J., Ehinger, K. A., Oliva, A., and Torralba, A. Sun database: Large-scale scene recognition from abbey to zoo. In *2010 IEEE computer society conference on computer vision and pattern recognition*, pp. 3485–3492. IEEE, 2010.

Zhang, C., Ren, H., and He, X. P^2ot: Progressive partial optimal transport for deep imbalanced clustering. *arXiv preprint arXiv:2401.09266*, 2024.

Zhou, K., Yang, J., Loy, C. C., and Liu, Z. Learning to prompt for vision-language models. *International Journal of Computer Vision*, 130(9):2337–2348, 2022.

Appendix

The appendix contains glossary, algorithm details, proofs, and detailed experimental results. The glossary contains a convenient reminder of our terminology (Appendix A). Appendix B provides more related works and discussion about the relationship between our work and related papers. Appendix C describes the relevant algorithms used in our experiments, including Prior Matching (Liusie et al., 2023) and BBSE (Lipton et al., 2018b). Appendix D provides the proofs of theorems that appeared in Section 4. Finally, we give more details and analysis of the experiments and provide additional experiment results in Appendix E

A. Glossary

The glossary is given in Table 2 below.

Symbol	Definition
n	Number of points
K	Number of classes
$[K]$	The set of classes $\{1, 2, \dots, K\}$
$\mathcal{X}$	Input feature space
$\mathcal{Y}$	Label space
X	Input features
Y	True labels
P_s	Source (training) distribution of data
P_t	Target (testing) distribution of data
s_θ	Prediction score function with parameter θ
C^*	Bayes optimal cost matrix for prediction
$\hat{C}$	Estimate of cost matrix for prediction
ν	Class balance for true labels
ν^{ZS}	Class balance for predicted labels from the zeroshot model
Δ_C	Additive perturbations to cost matrix
Δ_ν	Additive perturbation to class balance
π	Optimal transport plan
G, g	Constraint matrix and vector for linear programming s.t. feasible set is $\{x \in \mathcal{X} : Gx \geq g\}$
w	Dual solution for linear programming problem
κ	Hoffman constant for the true optimal transport problem
$[x]_+$	Take the positive parts of x, i.e. $[x]_+ := x\mathbb{1}[x > 0]$
$[x]_-$	Take the negative parts of x, i.e. $[x]_- := x\mathbb{1}[x < 0]$
$\text{vec}(A)$	Vectorized A, $\text{vec}(A) = [A_{11}, \dots A_{m1}, A_{12}, \dots, A_{m2}, \dots, A_{1n}, \dots A_{mn}]^T$ for $A \in^{m \times n}$

Table 2. Glossary

B. Background and Extended Related Work

B.1. Background

We briefly describe zero-shot models, the technical tool we use (optimal transport), along with other techniques that seek to address shifts.

Zero-shot Models. Zero-shot classification, popularized by models such as CLIP (Radford et al., 2021), is a powerful paradigm that enables prediction on downstream tasks without additional fine-tuning. Image, language, and multimodal models have been increasingly employed for zero-shot prediction (Wei et al., 2021; Liu et al., 2023). These models undergo extensive pretraining on massive datasets with concept and label spaces that may be very different from those of downstream applications.

Optimal Transport. Optimal Transport (OT) is a framework for matching two probability distributions (Peyré et al., 2019; Santambrogio, 2015). We predominantly consider optimal transport between empirical discrete measures. Suppose that we are given points $x_1, x_2, \ldots, x_n \in \mathcal{X}$ and $y_1, \ldots, y_K \in \mathcal{Y}$, a source measure μ defined by $\mu = \sum_{i=1}^{n} w_i \delta_{x_i}$, and a target measure given by $\nu = \sum_{j=1}^{K} p_j \delta_j$, where w_i, p_j are positive values such that $\sum_{i=1}^{n} w_i = 1$, $\sum_{j=1}^{K} p_j = 1$. Suppose also that δ_x is a Dirac delta function at x, i.e. $\delta_x(x') = 1$ if $x = x'$, and $\delta_x(x') = 0$ otherwise. Given a cost matrix $C \in \mathbb{R}^{n \times K}$, the Monge-Kantorovich formulation of optimal transport is to find a minimal cost transport plan π such that

$$\pi = \underset{\gamma \in \Pi(\mu,\nu)}{\arg\min} \langle \gamma, C \rangle,$$

where $\Pi(\mu, \nu) = \{\gamma \in \mathbb{R}_{+}^{n \times K} | \gamma \mathbf{1} = \mu, \gamma^T \mathbf{1} = \nu\}$.

Distribution and Label Shifts. Distribution shift refers to the discrepancy between a source distribution P_s on which the model is trained, and a target distribution P_t on which the model is deployed. Distribution shift often degrades trained model performance on target tasks. Label shift is a specific type of distribution shift such that $P_s(Y) \neq P_t(Y)$ and the data generation process is fixed — in other words, the conditional distributions of the inputs are the same: $P_s(X|Y) = P_t(X|Y)$. Techniques such as importance sampling (Lipton et al., 2018b; Azizzadenesheli et al., 2019; Garg et al., 2020), recalibration (Alexandari et al., 2020) and domain adaptation (Tachet des Combes et al., 2020) are commonly used to mitigate the effects of label shift. Unfortunately, these methods assume access to source distribution data, whereas zero-shot models' pretraining data is inaccessible (often proprietary or blocked for privacy reasons). Thus, adapting zero-shot models to new label distributions poses challenges unmet by these pre-existing methods.

B.2. Extended Related Work

Improving Zero-shot Classification at Inference Time. As zero-shot classification has gained popularity, several works have been developed to improve zero-shot classification at inference time. Chuang et al. (2023); Adila et al. (2023) use vector projection methods to remove spurious correlations at inference time. Menon & Vondrick (2022); Novack et al. (2023); An et al. (2023) augment prompts with language models and combine their classification output to improve zero-shot performance. Roberts et al. (2023) uses additional information of label space geometry to extend model pre-trained on the label subset to broader use-cases. While these works try to improve zero-shot classification at inference time in common, the main difference is that our method tackles the inherent class prior of zero-shot models.

Label Shift Adaptation. Label shift adaptation methods are designed to address the negative impacts arising from changes in the label distribution. These methods typically follow a two-step process (Lipton et al., 2018b; Azizzadenesheli et al., 2019; Garg et al., 2020). The first step involves estimating the label distribution within the target dataset using labeled data from the source distribution and unlabeled data from the target distribution. Next, the prediction scores are reweighted using the estimated target label distribution and the source label distribution. However, the standard approach requires access to the labeled source distribution data, which is usually not possible in zero-shot classification scenarios. OTTER provides a solution decoupled from the source data distribution, overcoming this limitation.

Improving Zero-shot Classification using Prior. Several studies have explored leveraging prior information to enhance zero-shot classification, even in the absence of access to source distributions. In the context of prompt-based zero-shot models, prior matching (Liusie et al., 2023) employs word prior distribution to alleviate word bias inherent in pretraining data. We adopted their adaptation method as a baseline. Similarly, Kahana et al. (2022) develop adaptation layers trained using priors, aiming to maintain proximity to the original scores. However, both approaches entail training additional layers and necessitate hyperparameter tuning, which may pose challenges in the context of zero-shot predictions. In contrast, OTTER presents a straightforward and efficient adaptation method to new label distributions without the need for any hyperparameter tuning, backed by theoretical guarantees.

Leveraging Optimal Transport for Enhanced Pseudo-labeling and Classification. A number of studies have explored the enhancement of pseudo-labeling and classification tasks through optimal transport, using label distribution specifications, in a similar spirit to our work, but within different contexts. Tai et al. (2021) uses optimal transport to allocate pseudo-labels to unlabeled datasets based on the label distribution specification in the semi-supervised setup. Wang et al. (2022) deals with long-tail distribution in the partial-label learning setup based on optimal transport. Zhang et al. (2024) uses partial optimal transport as a pseudo-labeling based approach for deep imbalanced clustering, progressively expanding the labeled sample proportion. Guo et al. (2022) reweights the training dataset to match the label distribution specification using optimal transport. This work mainly deals with the class imbalance problem in the training step. Shi et al. (2024) studies

classification from a matching perspective, revealing the connection between softmax loss and inverse optimal transport and suggesting a new loss function to address long-tail distributions. Their analysis provides useful insights for OTTER — why cost matrix induced by pre-trained models can be useful in the inference step. Xian et al. (2023) uses optimal transport as a postprocessing method to guarantee demographic parity. While sharing aspects of the approach, our work addresses class bias in zero-shot models. Peng et al. (2021) used optimal transport to handle long-tail recognition with a learned cost matrix. Our study provides a theoretical basis for understanding their empirical results. Chang et al. (2022) employs optimal transport to detect common and private classes between the source and the target domain, under the universal domain adaptation setting, where knowledge is transferred from source to target domain without any constraints on the label sets. In the context of zero-shot classification, there is no need to manage label space disparities between the source and target domains. Instead, the main concern of zero-shot classification is dealing with the distribution shift between the pretraining dataset and the downstream task. We tackle the label distribution shifts using optimal transport.

Class Imbalance. Class imbalance problems occur when the number of instances across different classes in a dataset is disproportionately distributed. This imbalance can severely bias the traininig process of a machine learning model, leading to poor generalization performance, especially for the minority classes. It has been extensively studied in the context of traditional machine learning (Fernández et al., 2018). Oversampling (Chawla et al., 2002) and cost-sensitive learning (Thai-Nghe et al., 2010) are well-known approaches to address class imbalance. Nonetheless, the inherent nature of class imbalance in pretraining datasets introduces a distinct set of challenges, especially when attempting to rectify such biases within the context of zero-shot classification scenarios.

C. Algorithm details

A toy example of label refinement by OTTER. To illustrate the benefits of OTTER, consider the following example for binary classification. We have two datapoints, $X = \{x_1, x_2\}$ with $Y = \{1, 2\}$, and true label distribution $\nu = (\frac{1}{2}, \frac{1}{2})$. Suppose that the zero-shot model's prediction scores are $s_1 = (0.4, 0.6)$ and $s_2 = (0.1, 0.9)$.

Traditional classification yields $\hat{y}_1 = 2, \hat{y}_2 = 2$, producing a 50% error rate. However, given the cost matrix C derived from the prediction score matrix

$$S = \begin{bmatrix} 0.4 & 0.6 \\ 0.1 & 0.9 \end{bmatrix}, C = \begin{bmatrix} -\log 0.4 & -\log 0.6 \\ -\log 0.1 & -\log 0.9 \end{bmatrix},$$

along with $\mu = (0.5, 0.5)$ and $\nu = (0.5, 0.5)$, the optimal transport procedure discovers the transport map $\pi = \begin{bmatrix} 0.5 & 0.0 \\ 0.0 & 0.5 \end{bmatrix}$, yielding $\hat{y}_1 = 1, \hat{y}_2 = 2$. This corrects the original zero-shot prediction error.

Prior matching (Liusie et al., 2023) proposed prior matching as a reweighting method for prompt-based classifiers to mitigate word bias — the distribution shift between pretrained language models' word prior and the class priors in the downstream task. We use it as a zero-shot model adaptation method given a class balance estimation.

Define reweighted probability scores of P_θ with r as $P_{\theta,r}(Y = j|X = x_i) = \dfrac{r_j P_\theta(Y = j|X = x_i)}{\sum_{j'=1}^{K} r_{j'} P_\theta(Y = j'|X = x_i)}$. Ideally, we hope to estimate the weight vector $r^* \in \mathbb{R}^n$ such that reweighted scores $P_{\theta,r^*}(Y = j|X = x_i)$ maximizes the accuracy in the target distribution. Since the labels are not given, this is impossible. Instead, prior matching matches the label distribution of predicted classes with the class balance estimate $\hat{\nu}$, i.e.

$$\hat{r}_j = \arg\min_{r_j \in \mathbb{R}} \left| \sum_{i=1}^{n} P_{\theta,r}(Y = j|X = x_i) - \nu_j \right|.$$

Though this is a non-convex optimization problem, it can be solved using the standard optimization techniques — we used (Loshchilov & Hutter, 2018). While this is equivalently effective with OTTER when properly optimized, we found that the temperature parameter and learning rate crucially affect the final accuracy, making it less ideal for the zeroshot adaptation. We used the grid search with the small validation set (10 samples per class) in each task to select hyperparameters. The hyperparameter ranges are as follows.

- Temperature: [1e-3, 1e-4, 1e-5, 1e-6, 1e-7]
- Learning rate: [1e-3, 1e-4, 1e-5, 1e-6, 1e-7]

Algorithm 2 Black Box Shift Estimator (BBSE)

Input: Source input data $\mathbf{X^s} = \{x_1^s, \ldots, x_m^s\}$, Source labels $\mathbf{Y^s} = \{y_1^s, \ldots, y_m^s\}$, Target input data $\mathbf{X^t} = \{x_1^t, \ldots, x_n^t\}$, model prediction distribution P_θ

Estimate the source class balance ν^s such that $\nu_j^s = \dfrac{\sum_{i=1}^n P_\theta(Y=j|X=x_i^s)}{m}$

Compute the naive target class balance $\tilde{\nu}^t$ such that $\tilde{\nu}_j^t = \dfrac{\sum_{i=1}^n P_\theta(Y=j|X=x_i^t)}{n}$

Estimate confusion matrix V such that $A_{jk} = \dfrac{1}{m}\sum_{i=1}^m P_\theta(Y=k|X=x_i^s)$

Estimate the refined target class balance $\hat{\nu}^t = A\tilde{\nu}^t$

Return $\hat{\nu}$

Black Box Shift Estimation (BBSE) Label shift adaptation methods (Lipton et al., 2018b; Azizzadenesheli et al., 2019; Garg et al., 2020) aims to estimate the class balance in the target distribution using the labeled source distribution data and the unlabeled target distribution data. We use Black Box Shift Estimation (BBSE) to estimate the class balance in the downstream task. Algorithm 2 describes the procedure. Note that the derivation of this algorithm depends on the label shift assumptions, thus the class balance estimation with the reference data or the synthetic data can be heavily biased.

D. Theory details

D.1. Classification as optimal transport.

Prior to discussing the main theoretical results, we demonstrate that standard classification—expressed as $\hat{y}_i = \arg\max_{j\in[K]} P_\theta(Y=j|X=x_i)$—can be interpreted as a (trivial) solution derived from optimal transport.

Theorem 4.1 (Classification as optimal transport)**.** *Let $\nu_j^{ZS} = \frac{1}{n}\sum_{i=1}^n \mathbb{1}[\hat{y}_i^{ZS} = j]$, where $\hat{y}_i^{ZS} = \arg\max_{j'\in[K]} P_\theta(Y = j'|X = x_i)$. Then, given $C_{ij} = -\log P_\theta(Y = j|X = x_i), \pi = \arg\min_{\gamma\in\Pi(\mu,\nu^{ZS})} \langle\gamma, C\rangle, \hat{y}_i^{OT} = \arg\max_{j\in[K]} \pi_{ij}$. Assuming there are no ties in scores, i.e. $P_\theta(Y = j|X = x_i) \neq P_\theta(Y = j'|X = x_i)$, for all $j \neq j'$, the predictions are equivalent, i.e. $\hat{y}_i^{OT} = \hat{y}_i^{ZS}$ for all $i \in [n]$.*

Proof of Thoerem 4.1. Suppose $\hat{y}_i^{OT} \neq \hat{y}_i^{ZS}$ for some $i \in [n]$. It implies $\sum_{i=1}^n -\log P_\theta(Y = \hat{y}_i^{OT}|X = x_i) < \sum_{i=1}^n -\log P_\theta(Y = \hat{y}_i^{ZS}|X = x_i)$. However, this is a contradiction since, for any $i \in [n]$, $\hat{y}_i^{ZS} = \arg\max_{j\in[K]} P_\theta(Y = j|X = x_i)$, thus $-\log P_\theta(Y = \hat{y}_i^{ZS}|X = x_i) \leq -\log P_\theta(Y = j|X = x_i)$ for all $j \in [K]$. □

This theorem has the following implications. First, it suggests that the predictions will remain unchanged if we set $\hat{\nu} = \nu^{ZS}$. Second, Bayes-optimal classifiers can be derived through optimal transport, using a (true) cost matrix defined as $C_{ij}^* = -\log P_t(Y = j|X = x_i)$, coupled with the true label distribution ν^*.

Our analysis begins with the label shift setup, which is a commonly-studied type of distribution shift—as well as a prominent issue when applying zero-shot models. We demonstrate that when the label distribution is correctly specified, optimal transport preserves the Bayes-optimal classifier predictions under label shift. Next, we consider general perturbations in label distribution and cost matrix as well as their impact on the resulting solutions.

D.2. Label Shift Invariance

In this setting, we assume features follow the same conditional distribution across source and target distributions, i.e. $P_s(X|Y) = P_t(X|Y)$. Furthermore, we suppose that the prediction scores are accurately calibrated in the training dataset, such that $s_\theta(x, j) = P_s(Y = j|X = x)$. For zero-shot models, we often lack access to P_s. This is a typical scenario in zero-shot model applications: after training on large-scale corpora, we use the pretrained model without the source dataset.

For a given downstream task with the target label distribution $\nu^* = P_t(Y)$, one standard approach to achieve the Bayes-optimal classifier for the target distribution is to reweight the score function outputs using the ratio $\frac{P_t(Y=j)}{P_s(Y=j)}$. This adjustment leads to:

$$\tilde{s}_\theta(x, j) = s_\theta(x, j) \cdot \frac{P_t(Y = j)}{P_s(Y = j)} \propto P_t(X = x|Y = j) \cdot P_t(Y = j) \propto P_t(Y = j|X = x).$$

This reweighted score function aligns with the target distribution, thus correcting label shift.

Although reweighting the score function is a popular solution, it faces an important obstacle when applied to zero-shot models like CLIP, where the source distribution $P_s(Y)$ is typically unknown. We show that OTTER successfully induces a Bayes classifier for the target distribution, represented as $f_t(x) = \arg\max_{j\in[K]} P_t(Y = j|X = x)$, without requiring access to $P_s(Y)$. This capability is particularly significant for zero-shot models, enabling them to adapt to target distributions effectively, even in the absence of explicit knowledge of the source distribution.

Now, we show that optimal transport can be an effective tool to correct label shift.

Theorem 4.2 (Label shift invariance)**.** *Suppose the pretrained model is well-calibrated for the source distribution,*

$$P_\theta(Y = j|X = x_i) = P_s(Y = j|X = x_i)$$

and there is no tie probability, for all $j \neq j', i \in [n]$

$$P_\theta(Y = j|X = x_i) \neq P_\theta(Y = j'|X = x_i).$$

Denote the Bayes optimal predictions in the target distribution as $\hat{y}_i^* = \arg\max_{j\in[K]} \log P_t(Y = j|X = x_i)$. Then OTTER *predictions* $\text{OTTER}(\mathbf{X}, P_t(Y), C)$ *are the same as Bayes optimal predictions $\hat{y}^*$.*

That is, OTTER recovers a Bayes classifier in the target distribution without access to the source distribution, given the target distribution and a well-calibrated model for the source dataset.

To prove Theorem 4.2, we show a specific form of invariance property of optimal transport first.

Theorem D.1. *Suppose $\pi^* = \arg\min_{\gamma\in\Pi(\mu,\nu)} \langle\gamma, C\rangle$ and E is a columnwise perturbation, i.e.,*

$$E = \begin{bmatrix}\epsilon_1\mathbf{1} & \epsilon_2\mathbf{1} & \cdots\epsilon_K\mathbf{1}\end{bmatrix},$$

where $\mathbf{1}$ denotes n dimensional vectors and $\epsilon_1, \ldots, \epsilon_K$ are constants. Then the perturbed cost matrix $\tilde{C} = C + E$, then π^* is also an optimal transport map with respect to the cost matrix $\tilde{C}$.

Proof. By the optimality condition, we have

$$\sum_{i,j} \pi_{ij}^* C_{ij} \leq \sum_{i,j} \pi_{ij} C_{ij}$$

for any $\pi \in \Pi(\mu, \nu)$. Then,

$$\sum_{i,j} \pi_{ij}^* C_{ij} + \sum_{j=1}^{K} \nu_j\epsilon_j \leq \sum_{i,j} \pi_{ij} C_{ij} + \sum_{j=1}^{K} \nu_j\epsilon_j,$$

which is

$$\sum_{i,j} \pi_{ij}^* C_{ij} + \sum_{j=1}^{K}\sum_{i=1}^{n} \pi_{ij}^*\epsilon_j \leq \sum_{i,j} \pi_{ij} C_{ij} + \sum_{j=1}^{K}\sum_{i=1}^{n} \pi_{ij}\epsilon_j.$$

Thus,

$$\sum_{i,j} \pi_{ij}^* \tilde{C}_{ij} \leq \sum_{i,j} \pi_{ij} \tilde{C}_{ij}.$$

□

This theorem is also valid for row-wise perturbations as well with a similar proof. Consequently, a straightforward implication is that

Corollary D.2. *Suppose $\pi^* = \arg\min_{\gamma\in\Pi(\mu,\nu)} \langle\gamma, C\rangle$, E is a columnwise perturbation and F is a row-wise perturbation, such that*

$$E = \begin{bmatrix}\epsilon_1\mathbf{1} & \epsilon_2\mathbf{1} & \cdots\epsilon_K\mathbf{1}\end{bmatrix},$$

$$F = \begin{bmatrix} \eta_1 \mathbf{1}^T \\ \eta_2 \mathbf{1}^T \\ \cdots \\ \eta_K \mathbf{1}^T \end{bmatrix},$$

where $\mathbf{1}$ *denotes* n *dimensional vectors with 1s, and* $\epsilon_1, \ldots, \epsilon_K, \eta_1, \ldots, \eta_K$ *are constants. Suppose the perturbed cost matrix is defined as* $\tilde{C} = C + E + F$*, then* π^* *is also an optimal transport map with respect to the perturbed cost matrix* $\tilde{C}$*.*

Now we provide the proof of Thoerem 4.2.

Proof of Theorem 4.2. Given

$$C_{ij} = -\log P_\theta(Y = j|X = x_i) = -\log P_s(Y = j|X = x_i),$$

the posteriors in the target distribution can be defined as $C^*_{ij} = -\log P_t(Y = j|X = x_i)$. From

$$P_t(Y = j|X = x_i) = P_s(Y = j|X = x_i)\frac{P_s(X = x_i)P_t(Y = j)}{P_t(X = x_i)P_s(Y = j)},$$

we can see that

$$\begin{aligned} C^*_{ij} &= -\log P_t(Y = j|X = x_i) \\ &= -\log P_s(Y = j|X = x_i)\frac{P_s(X = x_i)P_t(Y = j)}{P_t(X = x_i)P_s(Y = j)} \\ &= -\log P_s(Y = j|X = x_i) + \log P_s(Y = j) \\ &\quad - \log P_t(Y = j) - \log P_s(X = x_i) + \log P_t(X = x_i) \\ &= C_{ij} + E_{\cdot j} + F_{i\cdot} \end{aligned}$$

where $E_{\cdot j} = \log P_s(Y = j) - \log P_t(Y = j)$, $F_{i\cdot} = -\log P_s(X = x_i) + \log P_t(X = x_i)$. And, assuming $\nu_j = \frac{1}{n}\sum_{i=1}^n \mathbb{1}[\hat{y}^*_i = j]$, where $\hat{y}^*$ is the Bayes classifier prediction such that

$$\begin{aligned} \hat{y}^*_i &= \arg\max_{j\in[K]} P_t(Y = j|X = x_i) \\ &= \arg\min_{j\in[K]} -\log P_t(Y = j|X = x_i), \end{aligned}$$

optimal transport solution

$$\pi^* = \arg\min_{\gamma\in\Pi(\mu,\nu)} \langle \gamma, C^* \rangle$$

gives Bayes classifier predictions by Theorem 4.1.

Finally, by Corollary D.2, we have

$$\pi^* = \arg\min_{\gamma\in\Pi(\mu,\nu)} \langle \gamma, C \rangle = \arg\min_{\gamma\in\Pi(\mu,\nu)} \left\langle \gamma, \tilde{C} \right\rangle.$$

□

D.3. General Perturbation Sensitivity

In practical applications, calibration error could extend beyond noise in the elements of the cost matrix. A key source of error is label distribution estimation error. Hence, we address a more general setting, examining the impact of simultaneous perturbations in the label distribution and cost matrix of the transport plan. Our result applies techniques from perturbation theory for linear programming .

We rewrite our optimal transport problem $\min_{\pi\in\Pi(\mu,\nu)} \langle \pi, C \rangle$ as a linear programming problem. Let π and C be the transport plan and cost matrix respectively. Matrix G and vector g are used to denote the row and column constraints on π to

form a feasible plan which transports distribution from μ to ν.

$$H := \begin{bmatrix} \mathbf{1}_n^T \otimes \mathbb{I}_K \\ \mathbb{I}_n \otimes \mathbf{1}_K^T \end{bmatrix}, G = \begin{bmatrix} H \\ -H \end{bmatrix}, g = \begin{bmatrix} \mu \\ \nu \\ -\mu \\ -\nu \end{bmatrix}.$$

Then, we have the equivalent linear programming problem,

$$\min \left\{ \sum_{i,j} C_{i,j} \pi_{i,j} | G \cdot \text{vec}(\pi) \geq g, \pi \geq 0 \right\}. \tag{1}$$

We adapt a theorem from Robinson (1973) with our optimal transport problem notation.

Theorem D.3. *Let the primal linear programming problem be defined as in equation (1), and its dual problem be* $max\{w^T g | w^T G \leq vec(C)^T, w \geq 0\}$. *Suppose perturbed cost matrix is* $\hat{C} = C + \Delta_C$, *the perturbed class distribution* $\hat{\nu} = \nu + \Delta_\nu$, *such that* $\hat{g} = g + \Delta_g$ *where*

$$\Delta_g = \begin{bmatrix} 0 \\ \hat{\nu} - \nu \\ 0 \\ -\hat{\nu} + \nu \end{bmatrix}.$$

Assume that primal and dual problems are solvable. Denote the original solutions as π, w *and perturbed solutions as* $\hat{\pi}$ *and* $\hat{w}$. *Then,*

$$\left\| \begin{pmatrix} vec(\pi) \\ w \end{pmatrix} - \begin{pmatrix} vec(\hat{\pi}) \\ \hat{w} \end{pmatrix} \right\|_2 \leq \kappa(\|\Delta_\nu\|_2 + \|[vec(\Delta_C)]_+\|_2 + \|vec(C)^T vec(\hat{\pi}) - g^T \hat{w}\|_2),$$

where $1 \leq p \leq \infty$ *and* κ *is a Hoffman constant that only relates to the original problem (Hoffman, 1952).*

Ignoring the constant, the upper bound can be decomposed into three components,

- Δ_ν: noise (or the estimation error) of the target balance,
- $[\text{vec}(\Delta_C)]_+$: noise (or the calibration error) of the cost matrix,
- $\text{vec}(C)^T \text{vec}(\hat{\pi}) - g^T \hat{w}$: the suboptimality of perturbed solutions $\hat{w}, \text{vec}(\hat{\pi})$ in the original problem.

Theorem D.3 implies that the deviation from perturbed solution to true solution is bounded by the magnitude of perturbations and suboptimality of the perturbed solution. From this result, we can infer the following corollary and expect the prediction accuracy deteriorates given the perturbations of the label distribution and the calibration.

The proof of Theorem D.3 relies on the following result of (Robinson, 1973).

Lemma D.4 ((Robinson, 1973), Corollary 3.1.)**.** *Let the primal linear programming problem be*

$$\min_z \{p^T z | Gz \geqslant g, z \geqslant 0\}$$

and its dual be

$$\max_w \{w^T g | w^T G \leqslant p^T, w \geqslant 0\}.$$

Let $\bar{z}, \bar{w}$ *be the primal, dual solution. And, let the perturbed primal linear programming problem be*

$$\min_z \{\hat{p}^T z | \hat{G} z \geqslant \hat{g}, z \geqslant 0\}$$

and its dual be

$$\max_w \{w^T \hat{g} | w^T \hat{G} \leqslant \hat{p}^T, w \geqslant 0\}.$$

Let $\hat{z}, \hat{w}$ *be the corresponding primal, dual solution.*

Suppose that the primal and dual problems are solvable. Then,

$$\left\| \begin{pmatrix} \bar{z} \\ \bar{w} \end{pmatrix} - \begin{pmatrix} \hat{z} \\ \hat{w} \end{pmatrix} \right\|_2 \leq \kappa \left\| \begin{matrix} [(G-\hat{G})\hat{z} - (g-\hat{g})]^- \\ [(G-\hat{G})^T\hat{w} - (p-\hat{p})]^+ \\ (p-\hat{p})\hat{z} - (g-\hat{g})\hat{w} \end{matrix} \right\|_p ,$$

where $1 \leq p \leq \infty$ and κ is the Hoffmann constant determined by p, G, g. (Hoffman, 1952).

This Lemma provides a bound for error in the solution of the perturbed linear program. Since discrete optimal transport can be translated to standard linear program, we obtain Theorem D.3 by plugging in the definitions.

Proof of Theorem D.3 A discrete optimal transport problem

$$\min \left\{ \sum_{i,j} C_{i,j}\pi_{i,j} | \pi\mathbf{1} = \mu, \pi^T\mathbf{1} = \nu, \pi_{ij} \geq 0 \right\}$$

can be written as a linear program

$$\min\{p^T z | Gz \geqslant g, z \geqslant 0\},$$

where $p = vec(C)$, $z = vec(\pi), H = \begin{bmatrix} \mathbf{1}_n^T \otimes \mathbb{I}_K \\ \mathbb{I}_n \otimes \mathbf{1}_K^T \end{bmatrix}, G = \begin{bmatrix} H \\ -H \end{bmatrix}, g = \begin{bmatrix} \mu \\ \nu \\ -\mu \\ -\nu \end{bmatrix}$. Note that the equality constraints are converted to stacked inequalities. We have noisy cost matrix and label distribution in our setting, which leads to the perturbation on cost matrix C and ν such that the perturbed cost matrix is $\hat{C} = C + \Delta_C$, the perturbed label distribution $\hat{\nu} = \nu + \Delta_\nu$, such that $\hat{g} = g + \Delta_g$ where $\Delta_g = \begin{bmatrix} 0 \\ \hat{\nu} - \nu \\ 0 \\ -\hat{\nu} + \nu \end{bmatrix}$. Since we don't have perturbation on the constraint matrix G, $\hat{G} = G$. By plugging in these terms to Lemma D.4.

$$\begin{aligned}
\left\| \begin{pmatrix} \bar{z} \\ \bar{w} \end{pmatrix} - \begin{pmatrix} \hat{z} \\ \hat{w} \end{pmatrix} \right\|_2 &\leq \kappa \left\| \begin{matrix} [(G-\hat{G})\hat{z} - (g-\hat{g})]_- \\ [(G-\hat{G})^T\hat{w} - (p-\hat{p})]_+ \\ (p-\hat{p})\hat{z} - (g-\hat{g})\hat{w} \end{matrix} \right\|_2 \\
&= \kappa \left\| \begin{matrix} [g-\hat{g}]_- \\ [p-\hat{p}]_+ \\ (p-\hat{p})\hat{z} - (g-\hat{g})\hat{w} \end{matrix} \right\|_2 \\
&= \kappa \left\| \begin{matrix} 0 \\ [\hat{\nu}-\nu]_- \\ 0 \\ [\nu-\hat{\nu}]_- \\ [p-\hat{p}]_+ \\ p\hat{z} - g\hat{w} \end{matrix} \right\|_2 \qquad \because \text{ Optimality of } \hat{z}, \hat{w} \text{ in the perturbed problem.} \\
&= \kappa \left\| \begin{matrix} [\hat{\nu}-\nu] \\ [p-\hat{p}]_+ \\ p\hat{z} - g\hat{w} \end{matrix} \right\|_2 \\
&\leq \kappa \left(||(\Delta_\nu)||_2 + ||[vec(\Delta_C)]_+||_2 + \left|\left| vec(C)^T vec(\hat{\pi}) - g^T\hat{w} \right|\right|_2 \right).
\end{aligned}$$

We adapt the definition for the Hoffman constant from (Robinson, 1973). Computing Hoffman constant or even bounding it has been a long-standing problem (Azé & Corvellec, 2002; Pena et al., 2021; Peña, 2024). However, it has been shown that the Hoffman constant is a finite real number (Robinson, 1973), and specifically under our problem setup, it is independent

from perturbations and only related to original optimization problem. This suggests the possibility to regularize the parameters C, G, g in the original problem such that κ does not depend on the dimensionality of cost matrix or target distribution.

We first show a lemma to connect optimal transport plan with prediction accuracy. Let π and $\hat{\pi}$ be ground-truth and perturbed transport plan separately. Both transport plans are non-negative matrices of size $n \times K$, each row i contains one $1/n$ at column j and all other entries are zero, implying assigning the data point i to class j. Denote such classification rule as f_π and $f_{\hat{\pi}}$. By bounding L_2 error between the ground-truth and perturbed transport plan, we can infer the prediction accuracy of the perturbed transport plan as follows:

Corollary 4.1 (Suboptimality bound)**.** *Let the primal linear programming problem be defined as in equation (1), and its dual problem be $max\{w^T g | w^T G \leq vec(C)^T, w \geq 0\}$. Suppose perturbed cost matrix is $\hat{C} = C + \Delta_C$, the perturbed class distribution $\hat{\nu} = \nu + \Delta_\nu$, such that $\hat{g} = g + \Delta_g$ where*

$$\Delta_g = \begin{bmatrix} 0 \\ \hat{\nu} - \nu \\ 0 \\ -\hat{\nu} + \nu \end{bmatrix}.$$

Assume that primal and dual problems are solvable. Denote the original solutions as π, w and perturbed solutions as $\hat{\pi}$ and $\hat{w}$. Define the classification rule determined by transportation plan as f_π and $f_{\hat{\pi}}$. The prediction accuracy of the perturbed transport plan can be lower bounded as:

$$Acc(f_{\hat{\pi}}) = \sum_{i=1}^{n} \mathbf{1}[f_\pi(x_i) = f_{\hat{\pi}}(x_i)]/n \geq 1 - \frac{n\epsilon_n^2}{2},$$

where $\epsilon_n = \kappa(\|\Delta_\nu\|_2 + \|[vec(\Delta_C)]_+\|_2 + \|vec(C)^T vec(\hat{\pi}) - g^T \hat{w}\|_2)$.

Proof of Corollary 4.1. Since one wrong prediction in $\hat{\pi}$ induces $\sqrt{2/n^2}$ L_2 error between $vec(\pi)$ and $vec(\hat{\pi})$, an error bounded by ϵ suggests at most $\epsilon^2 n^2/2$ wrong predictions.

$$\begin{aligned} Acc(f_{\hat{\pi}}) &= \sum_{i=1}^{n} \mathbf{1}[f_\pi(x_i) = f_{\hat{\pi}}(x_i)]/n \\ &= (n - \sum_{i=1}^{n} \mathbf{1}[f_\pi(x_i) \neq f_{\hat{\pi}}(x_i)])/n \\ &\geq 1 - \frac{n\epsilon^2}{2}. \end{aligned}$$

Plugging in the transport plan error obtained from Theorem D.3 as ϵ, we can obtain the final prediction accuracy lower bound. □

D.4. Bounding label distribution estimation errors in few-shot learning

In few-shot learning, we assume that a few labeled samples per class are given. They can be used for estimating label distribution in the target distribution using label shift estimation methods (Lipton et al., 2018b; Azizzadenesheli et al., 2019; Garg et al., 2020). They comes with the sample complexity analysis under the label shift assumptions, which can be used to obtain bound the label distribution estimation errors.

Lemma D.5. *Let m and n denote the number of few-shot learning data and test datapoints, $w_i = \nu_i/\nu_i^s$ and $\hat{w}_i = \hat{\nu}_i/\nu_i^s$. Also let $\sigma_{\min}$ be the smallest eigenvalue of the covariance matrix $V_{\hat{y},y}$ where $[V_{\hat{y},y}]_{i,j} = P_s(f(x) = i, y = j)$. For $m > 80\log(m)\sigma_{\min}^{-2}$ and constant $c > 0$, the perturbation Δ_ν may be bounded as*

$$||\Delta_\nu||^2 \leq ||\nu^s||^2 \frac{c}{\sigma_{\min}^2} \left(||w||^2 \frac{\log m}{m} + K \frac{\log n}{n} \right),$$

with probability at least $1 - 3Km^{-10} - 2Kn^{-10}$.

The proof of Lemma D.5 relies on the following result of (Lipton et al., 2018a).

Lemma D.6. *Assume that*

1. $\forall x \in \mathcal{X}$ *and* $\forall y \in \mathcal{Y}$, $P_s(x|y) = P_t(x|y)$,
2. *if* $P_t(y) > 0$ *then* $P_s(y) > 0\ \forall y \in \mathcal{Y}$, *and*
3. *the expected confusion matrix* $C_s(f) = P_s(f(x), y) \in \mathbb{R}^{K\times K}$ *for classifier* f *is invertible.*

Then, there exists a constant $c > 0$ *such that for all* $m > 80\log(m)\sigma_{\min}^{-2}$, *with probability at least* $1 - 3Km^{-10} - 2Kn^{-10}$,

$$||\hat{w} - w||^2 \leq \frac{c}{\sigma_{\min}^2}\left(||w||^2\frac{\log m}{m} + K\frac{\log n}{n}\right).$$

Proof of Lemma D.5. Where all norms are Euclidean unless otherwise denoted, we have that

$$\begin{aligned}||\Delta_\nu||^2 &= ||\hat{\nu} - \nu||^2\\ &= ||\nu^s \otimes (\hat{w} - w)||^2\end{aligned}$$

for element-wise multiplication operation $\otimes$. Further,

$$\begin{aligned}||\nu^s \otimes (\hat{w} - w)||^2 &\leq ||\nu^s(\hat{w} - w)||_F^2\\ &\leq ||\nu^s||_2^2||\hat{w} - w||^2\\ &\leq ||\nu^s||^2\frac{c}{\sigma_{\min}^2}\left(||w||^2\frac{\log m}{m} + K\frac{\log n}{n}\right),\end{aligned}$$

where the last line follows from Lemma D.6 with probability at least $1 - 3Km^{-10} - 2Kn^{-10}$. □

D.5. Bounding the perturbation on cost matrix

Further, we can bound $[vec(\Delta_C)]_+$ by the Total Variation Distance (TVD) between P_s and P_θ as follows.

Lemma D.7. *Let* $\tau = \frac{1}{2}||P_s - P_\theta||_1$ *denote the Total Variation Distance between* P_s *and* P_θ *and define* $\min(C) = \min_{i,j} C_{ij}$. *Then,*

$$||[vec(\Delta_C)]_+|| \leq \sqrt{m(K-1)}\log\left(\frac{\tau}{\min(C)} + 1\right).$$

Proof of Lemma D.7. For each element $\Delta_C^{(ij)}$ of Δ_C, we have that

$$\begin{aligned}\Delta_C^{(ij)} &= \log P_\theta(Y = j|X = x_i) - \log P_s(Y = j|X = x_i)\\ &= \log\frac{P_\theta(Y = j|X = x_i)}{P_s(Y = j|X = x_i)}.\end{aligned}$$

For i, j such that $P_\theta(Y = j|X = x_i) \leq P_s(Y = j|X = x_i)$, clearly $\Delta_C^{(ij)} \leq 0$ and so $[vec(\Delta_C^{(ij)})]_+ = 0$.

Otherwise, for i, j such that $P_\theta(Y = j|X = x_i) > P_s(Y = j|X = x_i)$, it follows that $\Delta_C^{(ij)} > 0$ and

$$\begin{aligned}\Delta_C^{(ij)} &= \log\frac{P_\theta(Y = j|X = x_i) - P_s(Y = j|X = x_i) + P_s(Y = j|X = x_i)}{P_s(Y = j|X = x_i)}\\ &\leq \log\left(\frac{\tau}{P_s(Y = j|X = x_i)} + 1\right)\\ &\leq \log\left(\frac{\tau}{\min(C)} + 1\right).\end{aligned}$$

For each $i \in [m]$, there are at most $K-1$ possible j such that $P_\theta(Y=j|X=x_i) > P_s(Y=j|X=x_i)$, because $\sum_{j\in[K]} P_\theta(Y=j|X=x_i) = \sum_{j\in K} P_s(Y=j|X=x_i)$. Therefore, there are at most $m(K-1)$ pairs $(i,j) \in [m]\times[K]$ such that $0 < \Delta_C^{(ij)} \leq \log\left(\frac{\tau}{\min(C)}+1\right)$. Thus,

$$||[vec(\Delta_C)]_+|| \leq \sqrt{m(K-1)}\log\left(\frac{\tau}{\min(C)}+1\right).$$

□

	CIFAR10	CIFAR100	Caltech101	Caltech256	Food101	STL10
n	10,000	10,000	7,162	22,897	25,250	8,000
K	10	100	101	256	101	10
Imbalance	1.00	1.00	49.06	15.94	1.00	1.00
	SUN397	Flowers102	EuroSAT	Oxford-IIIT-Pet	STANFORD-Cars	Country211
n	87,004	6,149	22,000	3,669	8,041	211,00
K	397	102	10	37	196	211
Imbalance	25.43	11.90	1.67	1.14	2.83	1.00
	DTD	CUB	ImageNet	ImageNet-r	ImageNet-Sketch	
n	1,880	5,794	40,000	26,000	40,889	
K	47	200	1,000	200	1,000	
Imbalance	1.00	2.73	1.00	13.23	1.03	
	Amazon	Gender	CivilComments	HateXplain		
n	89,078	21,750	131,782	1,621		
K	2	2	2	3		
Imbalance	19.45	6.03	8.26	1.52		

Table 3. Statistics of the test dataset in each task. Class imbalance is measured by $\frac{\max_{j\in[K]} P_t(Y=j)}{\min_{j\in[K]} P_t(Y=j)}$.

E. Experiment details

E.1. Datasets

Zeroshot image classification datasets We use CIFAR10, CIFAR100 (Krizhevsky et al., 2009), Caltech101 (Fei-Fei et al., 2006), Caltech256 (Griffin et al., 2007), Food101 (Bossard et al., 2014), STL10 (Coates et al., 2011), SUN397 (Xiao et al., 2010), Flower102 (Nilsback & Zisserman, 2008), EuroSAT (Helber et al., 2019), Oxford-IIIT Pet (Parkhi et al., 2012), Stanford Cars (Krause et al., 2013), DTD (Cimpoi et al., 2014), CUB (Wah et al., 2011), ImageNet (Deng et al., 2009), ImageNet-r (Hendrycks et al., 2021), and ImageNet-Sketch (Wang et al., 2019).

Zeroshot text classification datasets We use Amazon (Ni et al., 2019), Gender (Dinan et al., 2020), CivilComments (Borkan et al., 2019), and HateXplain (Mathew et al., 2021).

Synthetic datasets Suppose $X|Y=0 \sim \mathcal{N}(-1,1)$ and $X|Y=1 \sim \mathcal{N}(1,1)$. Training data is sampled from a mixture of Gaussians $X_s \sim \nu_0^s\mathcal{N}(-1,1)+\nu_1^s\mathcal{N}(1,1)$ such that $P_s(Y=0)=\nu_0^s, P_s(Y=1)=\nu_1^s, \nu_0^s+\nu_1^s=1$. Similarly, we sample the test data from $X_t \sim \nu_0^t\mathcal{N}(-1,1)+\nu_1^t\mathcal{N}(1,1)$. We fix the training set label distribution as $\nu_0^s=0.1, \nu_1^s=0.9$ and vary test set label distribution ν^t to simulate label shift. We train a logistic regression model with 10,000 samples from the source distribution, and test the model with 10,000 samples from the target distribution. A Bayes-optimal classifier in the target distribution is given by $f_{Bayes}(x)=\mathbb{1}[x \geq \frac{1}{2}(\log\frac{\nu_0^t}{\nu_1^t}+1)]$. The naive classifier is defined as the maximizer of the predicted score. The OTTER predictions are produced with Algorithm 1, with the cost matrix $C_{ij}=-\log P_\theta(Y=j|X=x_i)$ and the label distribution specification ν^t, where $P_\theta(Y|X)$ represents the logistic regression model scores.

		CIFAR10	CIFAR100	Caltech101	Caltech256	Food101	STL	SUN397	Flower102
RN50	Zero-shot	66.5	38.70	74.7	74.1	76.3	93.1	57.8	57.3
	Prior Matching	76.4(±0)	41.1(±2.5)	44.3(±9.7)	9.8(±1.6)	77.5(±1.4)	94.7(±0)	12.3(±3.9)	50.0(±2.8)
	OTTER(Ours)	**76.8**	**44.6**	**83.6**	**80.2**	**81.1**	**95.5**	**63.8**	**64.3**
RN101	Zero-shot	79.1	46.3	81.6	77.7	80.9	96.5	55.6	61.1
	Prior Matching	80.3(±0.1)	46.7(±1.3)	57.6(±14.2)	9.6(±2.4)	80.8(±3.7)	96.7(±6)	17.6(±5)	49.0(±20.9)
	OTTER(Ours)	**81.1**	**50.9**	**88.8**	**83.6**	**84.4**	**97.2**	**63.8**	**67.7**
ViT-B/32	Zero-shot	88.9	58.5	81.3	79.5	80.2	97.1	61.1	59.3
	Prior Matching	**89.7**(±0)	58.1(±1.2)	54.7(±14.1)	9.5(±1.6)	80.0(±4.4)	97.4(±0)	11.3(±3.1)	51.5(±3.2)
	OTTER(Ours)	**89.7**	**64.4**	**88.1**	**84.9**	**85.0**	**97.8**	**68.0**	**68.1**
ViT-B/16	Zero-shot	88.3	63.9	81.0	81.1	85.6	98.0	62.8	63.9
	Prior Matching	91.3(±0)	64.1(±2.7)	59.3(±15.4)	9.5(±1.5)	86.8(±3.1)	98.4(±0)	6.7(±1.6)	54.0(±14.1)
	OTTER(Ours)	**91.7**	**67.9**	**88.7**	**87.0**	**89.9**	**98.6**	**70.4**	**70.8**
ViT-L/14	Zero-shot	95.0	72.3	80.3	85.0	89.8	99.2	64.9	72.3
	Prior Matching	95.2(±0)	73.5(±2.5)	68.5(±19.7)	9.4(±1.2)	90.4(±3.8)	99.3(±0)	26.5(±1.1)	66.5(±17.9)
	OTTER(Ours)	**96.0**	**77.7**	**92.0**	**90.9**	**93.6**	**99.4**	**71.5**	**81.3**

Table 4. CLIP Zero-shot image classification accuracy (%)

E.2. Zero-shot classification setup

Image zero-shot classification For zero-shot image classification, we emply CLIP (Radford et al., 2021) models. We used "a photo of a [CLASS]" prompt. Scores are computed by $s_\theta(x_i, j) = P_\theta(Y = j|X = x_i) = \frac{\exp\left(\cos(f(x_i), g(y_j))/\tau\right)}{\sum_{j'=1}^{K} \exp\left(\cos(f(x_i), g(y_{j'}))/\tau\right)}$ for image x_i regarding the label j, given the image encoder f, the text encoder g. Cost matrix is constructed by $C = [c_{ij}]_{i\in[n],j\in[K]}$, where $c_{ij} = -\log s_\theta(x_i, j)$. We run 1 with the true class balance of the test dataset.

Text zero-shot classification We employ BERT and text-embedding-ada-002 sentence embeddings for text classification (Reimers & Gurevych, 2019). This process parallels the methodology used in image zero-shot classification — we compute the prediction scores from the cosine similarity and then construct the cost matrix with the negative log probabilities.

E.3. Detailed experiment results of Section 5.1

Ablation on zero-shot models For the ablation study on zero-shot models, we provide experimental results with varying architectures, given the exact prior. Table 4, 5 show the image zero-shot classification results, and Table 6 shows the text zero-shot classification results. We also provide another baseline results with CLIPPR (Kahana et al., 2022), which uses the label distribution for adapter training. CLIPPR is similar with Prior Matching in the point that it requires adapter training, but it has more adapter layers and additional loss function to make the predictions stick to the original prediction scores. While the performance gain varies, we can observe that OTTER is effective for the most cases.

		EUROSAT	Pet	CUB	Stanford	Country211	CUB	ImageNet	ImageNet-r	Imagenet-Sketch
RN50	Zero-shot	18.2	80.5	45.6	13.3	37.3	47.1	51.5	34.9	5.3
	Prior Matching	**31.5**(±6)	77.4(±0.3)	27.5(±1.9)	13.1(±0.6)	41.6(±0.2)	36.(±0.1)	44.6(±0.1)	7.8(±1.8)	5.(±0)
	OTTER(Ours)	26.8	**83.0**	**49.2**	**14.1**	**42.2**	**51.7**	**54.1**	**37.1**	**5.7**
RN101	Zero-shot	33.8	80.2	52.8	14.8	37.3	50.1	53.4	41.4	6.5
	Prior Matching	**34.0**(±5.9)	77.2(±0.4)	34.8(±2.9)	15.1(±0.7)	39.4(±0.1)	33.6(±0.1)	46.7(±0.1)	9.5(±3.1)	6.5(±0.1)
	OTTER(Ours)	33.0	**84.2**	**55.2**	**16.0**	**40.7**	**52.7**	**56.0**	**43.7**	**7.4**
ViT-B/32	Zero-shot	29.7	81.7	49.0	15.5	40.7	51.4	55.6	60.7	34.3
	Prior Matching	41.2(±0.7)	77.5(±0.6)	31.5(±1.1)	14.8(±0.1)	42.9(±0.1)	36.3(±0.9)	48.3(±0.1)	11.7(±0.8)	30.4(±0.3)
	OTTER(Ours)	**44.9**	**86.2**	**52.10**	**15.9**	**45.1**	**54.7**	**57.7**	**64.2**	**39.4**
ViT-B/16	Zero-shot	32.9	83.8	55.7	19.8	39.0	55.3	60.3	68.4	39.9
	Prior Matching	41.6(±0.8)	82.(±0.3)	39.8(±2.6)	19.(±0.1)	42.1(±0.1)	40.4(±0)	53.6(±0.1)	16.6(±3.5)	36.5(±0.4)
	OTTER(Ours)	**42.0**	**88.8**	**59.7**	**21.2**	**44.4**	**58.4**	**62.9**	**71.8**	**44.7**
ViT-L/14	Zero-shot	25.75	87.93	64.12	28.2	50.8	61.8	67.6	80.6	51.9
	Prior Matching	**59.2**(±0.4)	84.(±0.5)	53.(±15.6)	27.5(±0.3)	**51.5**(±0)	43.9(±0.3)	62.3(±0.1)	17.6(±5.1)	47.2(±0.4)
	OTTER(Ours)	57.62	**91.03**	**70.02**	**29.5**	51.0	**66.3**	**70.2**	**83.3**	**55.2**

Table 5. CLIP Zero-shot image classification accuracy (%) continued.

		Amazon review	GenderBias	CivilComments	HateXplain
BERT	Zero-shot	74.0 (± 0.0)	84.1 (± 0)	48.4 (± 0.0)	30.9 (± 0.0)
	Prior matching	58.8 (± 46.4)	41.4 (± 39.6)	57.2 (± 37.7)	31.3 (±3.3)
	OTTER(Ours)	**91.7 (± 0.0)**	**91.9 (± 0.0)**	**81.4 (± 0.0)**	**34.3 (± 0.0)**
Ada	Zero-shot	72.3 (± 0.0)	50.9 (± 0.0)	56.2 (± 0.0)	27.9 (± 0.0)
	Prior matching	58.8 (± 43.7)	50.0 (± 41.3)	55.2 (± 35.5)	**32.4 (± 4.0)**
	OTTER(Ours)	**97.0 (± 0.0)**	**73.7 (± 0.0)**	**82.0 (± 0.0)**	32.0 (± 0.0)

Table 6. Text embedding zero-shot classification mean accuracy and standard deviation (%)

Ablation on the class balance specification We conducted a semi-synthetic experiment to investigate the sensitivity to the label distribution specification error in real datasets. We generate the noisy label distribution specification and see how the accuracy changes. We control the noise in the label distribution specification as follows. Given the true class balance ν^*, first we make adversarial class balance ν^{adv} such that $\nu^{adv}_{j^*} = 1$ for $j^* = \arg\min_{j\in[K]} \nu^*_j$ and $\nu^{adv}_j = 0$ for $j \neq j^*$. To measure distance between class balance specification and true class balance, we use the total variance $TV(\nu, \hat{\nu}) = \frac{1}{2}\,||\nu - \hat{\nu}||_1$. Next, we intepolate ν^* and ν^{adv} such that $TV(\nu^*, \nu^\alpha) = \alpha$, by $\nu^\alpha = (1 - \frac{\alpha}{TV(\nu^*,\nu^{adv})})\nu^* + \frac{\alpha}{TV(\nu^*,\nu^{adv})}\nu^{adv}$. We set the interval of alpha as 0.01 and vary it up to 0.2.

Figure 3 shows the result. We observe the sensitivity to the label distribution specification error varies depending on the datasets, but generally we can observe that the accuracy degrades linearly proportionally to the class balance error. While the result may vary depending on the interaction between class balance error and calibration error in cost matrix, we can expect performance improvement if the class balance specification is good enough.

Inference time comparison To show that the additional computation complexity induced by OTTER is not heavy, we measured the time consumption (in seconds) for the inference step in the experiments in Section 5.1, with the pre-computed embeddings. Table E.3 presents the result. Time reduction column represents the time reduction rate of OTTER compared to PM. Measurements were taken using a machine equipped with an Intel® Core™ i7-11700K @ 3.60GHz processor, 64GB RAM, and NVIDIA GPU RTX-4090. For most cases ($n < 30000$), our method takes less than 1 second, while the prior

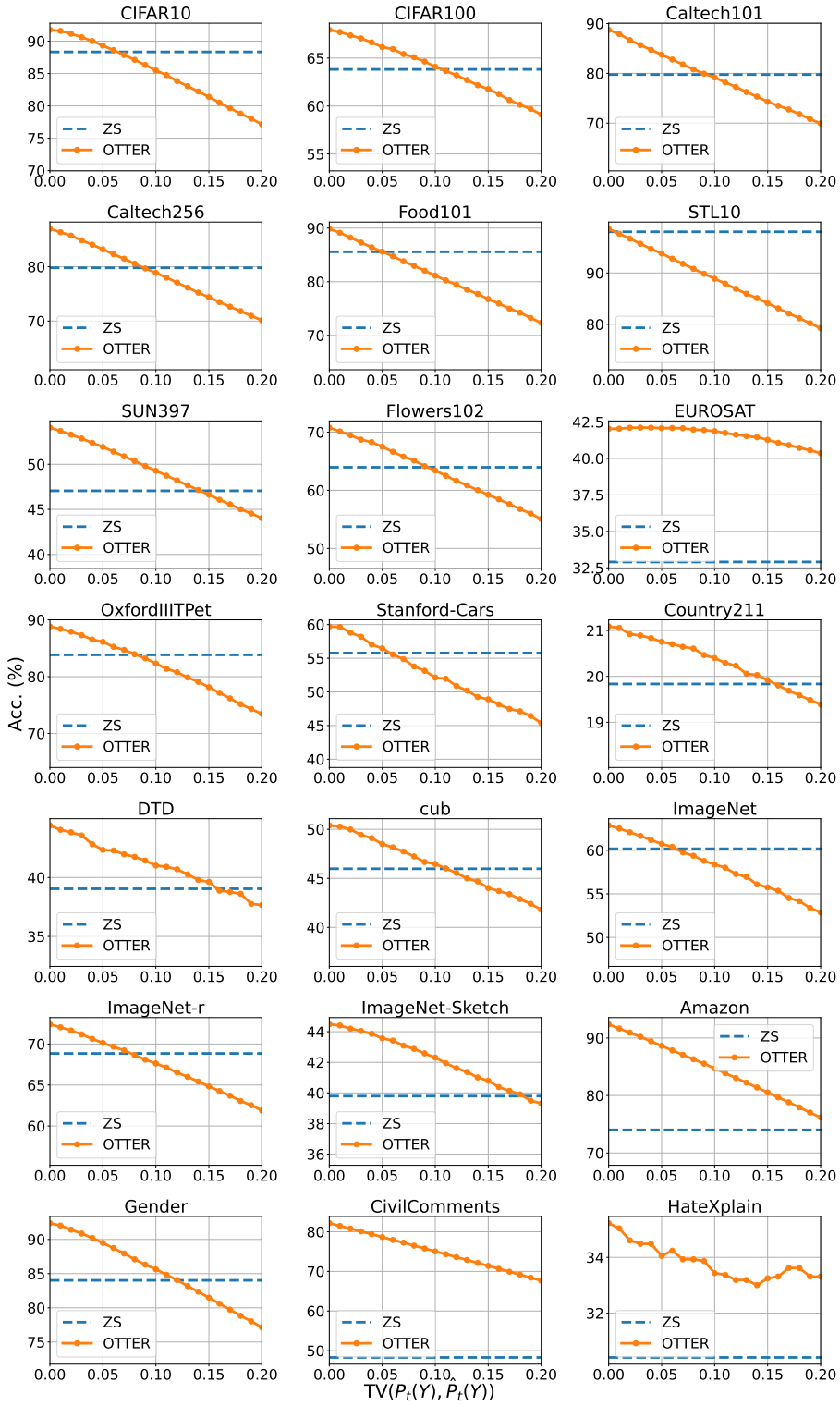

Figure 3. Ablation experiment on the class balance specification. X-axis represents the total variation distance between the class specification true class balance $P_t(Y)$ and $\hat{P}_t(Y)$. Y-axis represents accuracy. ViT-B/16 is used as the image zero-shot classifier, and BERT is used as the text zero-shot classifier.

Dataset	n	ZS	PM	OTTER	Time reudction (%)
CIFAR10	10000	0.0381	3.7127	0.0733	98.03
CIFAR100	10000	0.0462	3.6296	0.1947	94.64
Caltech101	7162	0.0298	3.6445	0.1188	96.74
Caltech256	22897	0.2111	3.9597	0.8568	78.36
Food101	25250	0.1186	3.6968	0.4969	86.56
STL10	8000	0.0304	3.4877	0.0546	98.43
SUN397	87004	1.1233	33.0386	10.5316	68.12
Flowers102	6149	0.0280	3.7216	0.0959	97.42
EuroSAT	22000	0.0826	3.6655	0.3491	90.48
OXFORD-IIIT-Pet	3669	0.0137	3.3901	0.0233	99.31
STANFORD-Cars	8041	0.0413	3.4910	0.1964	94.37
Country211	21100	0.1285	3.7665	1.0537	72.02
DTD	1880	0.0070	3.4603	0.0156	99.55
CUB	5794	0.0306	3.5583	0.1410	96.04
ImageNet	40000	0.9954	37.6932	8.1003	78.51
ImageNet-r	26000	0.1921	3.8331	0.9834	74.35
ImageNet-Sketch	40889	1.0189	38.4853	9.0579	76.46

Table 7. Inference time comparison with pre-computed embeddings (in seconds).

	ZS	PM	OT	ZS + CD	PM + CD	OT + CD
EuroSAT	32.90	11.36	42.03	53.62	11.37	**57.15**
Oxford-IIIT-Pet	83.84	23.11	88.83	87.95	16.33	**91.01**
DTD	39.04	8.83	**44.41**	42.87	14.73	43.24
CUB	45.98	10.34	50.40	55.51	11.49	**58.47**
ImageNet	60.18	12.42	62.86	66.46	14.08	**68.05**

Table 8. Accuracy in the prompt-enhanced zero-shot classification by Classification by Description (CD) (Menon & Vondrick, 2022). We can observe OTTER's capability to provide further enhancements upon refined the improvements achieved through refined prompts.

matching baseline takes more than 3 seconds. It's worth noting that the time consumption for computing embeddings is more substantial; even 10 seconds is negligible compared to the embedding time consumption (ranging from 5 to 30 minutes for each evaluation set), which is common for all inference conditions.

Ablation on prompts Recent studies have demonstrated the efficacy of enhancing prompts as a means to improve zero-shot models (Zhou et al., 2022; Menon & Vondrick, 2022). In order to further illustrate the potential enhancements offered by OTTER beyond enhanced prompts, we reproduced Menon & Vondrick (2022)'s approach (Classification by Description, CD), which employs multiple prompts generated by language models and takes max scores of them for each class. We applied OTTER to CD. The results of this experiment are summarized in Table E.3. As anticipated, OTTER exhibits enhancements in zero-shot classification, even when prompt sets are refined using language models.

E.4. Few-shot adaptation with label distribution estimation

Setup and Procedure. We use the same datasets as the previous experiment. We consider a 10-shot learning setting: 10 labeled samples per class are given. Note that labeled samples have uniform label distribution, while the label distribution in the target distribution *may not be uniform*. This setting requires the use of label distribution estimation methods used in label shift adaptation (Lipton et al., 2018b; Azizzadenesheli et al., 2019; Garg et al., 2020). We estimate the target label distribution with Black Box Shift Estimation (BBSE) (Lipton et al., 2018b). BBSE estimates the target balance using confusion matrix, under the label shift assumption. For detailed explanation, refer to Appendix C.

Expected Results. We expect OTTER can improve zero-shot classification if the label distribution estimation error is sufficiently small. Also, we expect OTTER can improve linear probing, which is one of standard approaches for few-shot learning.

Results. We found OTTER improves zero-shot text classifications where the number of classes is small ($K = 2$ or 3), and improves linear probing in image classification with a large number of classes. Table 9 shows the text zero-shot classification results. While it shows a relatively high variance due to the small sample size ($20 \sim 30$), the average accuracy significantly improves over zero-shot classification. Table 10 shows the linear probing experiment results. The result shows that OTTER can yield additional improvement upon linear probing. Full results that have both of zero-shot classification and linear probing are given in Appendix E.

	Zero-shot	Prior Matching	OTTER
Amazon review	74.0	47.9 (±45.5)	**89.9** (±11.1)
GenderBias	84.0	57.0 (±36.5)	**87.8** (±4.4)
CivilComments	48.4	**69.1** (±33.7)	55.81 (±17.9)
HateXplain	30.9	34.4 (±6.0)	**35.2** (±3.3)

Table 9. Accuracy (%) in zero-shot text classification with BERT. We use the label distribution estimation by BBSE for Prior Matching and OTTER. We report the mean and the standard deviation of 10 different samplings of the labeled data.

	LP	LP + PM	LP + OTTER
CIFAR10	**90.2** (±0.6)	89.8 (±1.1)	90.0 (±0.6)
CIFAR100	58.3 (±0.8)	24.4 (±12.2)	**60.5** (±0.6)
Caltech101	**91.5** (±0.8)	87.5 (±9.3)	91.4 (±0.9)
Caltech256	84.5 (±0.4)	58.4 (±23.5)	**85.4** (±0.4)
Country211	12.4 (±0.4)	9.2 (±2.4)	**13.2** (±0.3)
DTD	58.6 (±1.1)	49.0 (±9.3)	**59.3** (±1.1)
EUROSAT	74.6 (±1.4)	71.6 (±3.5)	**75.9** (±3.0)
Flowers102	89.0 (±0.0)	87.8 (±0.0)	**90.2** (±0.1)
Food101	79.1 (±0.9)	60.6 (±17.1)	**79.8** (±0.6)
Oxford-IIIT-Pet	**75.7** (±1.3)	72.0 (±8.8)	75.6 (±1.7)
Stanford-Cars	64.5 (±0.8)	65.4 (±0.9)	**66.3** (±0.8)
STL10	**97.7** (±0.6)	97.5 (±0.9)	97.6 (±0.5)
CUB	72.2 (±0.1)	63.3 (±23.0)	**75.6** (±0.4)
ImageNet	56.8 (±0.0)	53.6 (±4.1)	**59.8** (±0.0)
ImageNet-r	54.9 (±0.8)	47.6 (±11.0)	**57.1** (±0.8)
ImageNet-Sketch	43.4 (±0.0)	37.9 (±1.4)	**48.3** (±0.0)

Table 10. Accuracy (%) in linear probing image classification with ViT-B/16. We use the true label distribution as the label distribution specification. We report the mean and standard deviation of 10 different random samplings of the validation set. We excluded SUN397 since linear probing collapses.

Table 10 shows the experiment results. The result shows that OTTER can yield mild improvement over linear probing, even with the label distribution estimation errors. More detailed analysis regarding estimation erorr and the number of samples is provided in Appendix E.5.

E.5. Detailed experiment results of Section E.4

Class balance estimation errors We report the class balance errors in Section E.4. As a metric, we use the total variance $TV(\nu, \hat{\nu}) = \frac{1}{2} ||\nu - \hat{\nu}||_1$. We use zeroshot prediction scores and linear probing prediction scores for BBSE. $\hat{\nu}^{zs}$ denotes the

Dataset	TV($\nu^*, \hat{\nu}^{zs}$)	TV($\nu^*, \hat{\nu}^{lp}$)	Dataset	TV($\nu^*, \hat{\nu}^{zs}$)	TV($\nu^*, \hat{\nu}^{lp}$)
CIFAR10	0.071	**0.038**	STL10	0.021	**0.011**
CIFAR100	0.219	**0.153**	SUN397	0.503	**0.458**
Caltech101	0.130	**0.041**	CUB	0.245	**0.102**
Caltech256	0.126	**0.081**	ImageNet	**0.175**	**0.175**
Country211	0.439	**0.336**	ImageNet-r	0.210	**0.189**
DTD	0.441	**0.160**	ImageNet-sketch	0.236	**0.211**
EUROSAT	0.404	**0.084**	Amazon	**0.090**	0.253
Flowers102	0.202	**0.067**	CivilComments	**0.369**	0.383
Food101	0.112	**0.090**	Gender	**0.083**	0.155
Oxford-IIIT-Pet	0.219	**0.114**	HateXplain	0.253	**0.203**
Stanford-Cars	0.255	**0.143**			

Table 11. Class balance estimation error with BBSE in Section E.4. We report the mean of 10 different random samplings of the validation set. Lower is better.

estimated class balance based on zero-shot prediction scores, and $\hat{\nu}^{lp}$ represents the estimated class balance based on linear probing prediction scores.

Table 11 shows the result. We can see that total variation decreases with linear probing in image classification tasks since they reduces the violation of label shift assumptions. However, total variation increases in text classification tasks due to the small number of labeled sample size, following the size of label space ($K = 2$ or 3). Accordingly, we can expect OTTER will be more useful with linear probing, and just rebalancing zero-shot predictions with OTTER could be enough for text classification tasks.

Ablation experiments on linear probing We provide full results of Section E.4. Specifically, we additionally report the results of combination with linear probing in text classification tasks and the results of zero-shot classification results in image classification tasks.

The results are presented in Table 12. While OTTER often provides additional improvement over LP, zero-shot classification was a strong baseline in image classification tasks. Meanwhile, class balance adaptation in text classification tasks is effective in all cases, giving a significant improvement over zero-shot predictions.

Ablation experiments on the number of examples per class Few-shot adaptation scenario assumes we have access to labeled data to estimate the target distribution. We hypothesize that an increase in the number of labeled samples enhances the accuracy of the class balance estimation, thereby improving the performance of OTTER. To test this hypothesis, we use few-shot adaptation in image and text classification tasks, without linear probing. The experiment varies the number of samples per class from 10 to 100, anticipating a reduction in class balance estimation error and an improvement in OTTER's accuracy with the increase in labeled samples.

The results, as depicted in Figure 4, corroborate our hypothesis. It is evident that the error in class balance estimation diminishes with an increasing number of samples, leading to a concurrent enhancement in the accuracy of OTTER.

Comparison between OTTER and Linear Probing with varying number of classes In the few-shot adaptation scenario, we explored three approaches: OTTER, linear probing (LP), and a combination of LP + OTTER. We formulated two hypotheses. The first posits that OTTER might outperform LP, particularly in situations with a limited number of samples. The second hypothesis suggests that OTTER could provide further enhancements to LP even when LP already surpasses the naive version of OTTER. This experiment was conducted using the same setup as the previous one.

The results, displayed in Figure 5, reveal several insights regarding our hypotheses. To begin with, OTTER demonstrates performance on par with LP, especially in scenarios with fewer samples. Interestingly, OTTER achieves superior accuracy compared to LP in datasets like Amazon and CivilComments, characterized by a small number of classes ($K = 2$), resulting in a relatively low total sample count. Furthermore, it is observed that incorporating OTTER into LP leads to an average increase in accuracy.

Dataset	ZS	ZS BBSE+PM	ZS BBSE+OT	LP	LP BBSE+PM	LP BBSE+OT
CIFAR10	88.3	72.7	87.5	**90.2**	89.8	90.0
CIFAR100	**63.8**	3.2	59.1	58.3	24.4	60.5
Caltech101	79.8	32.5	80.7	**91.5**	87.5	91.4
Caltech256	79.8	6.0	80.3	84.5	58.4	**85.4**
Country211	**19.8**	1.5	15.9	12.4	9.2	13.2
DTD	39.0	3.2	31.2	58.6	49.0	**59.3**
EUROSAT	32.9	19.2	34.0	74.6	71.6	**75.9**
Flowers102	64.0	40.3	60.8	89.0	87.8	**90.2**
Food101	**85.6**	15.3	82.3	79.1	60.6	79.8
Oxford-IIIT-Pet	**83.8**	43.3	71.4	75.7	72.0	75.6
Stanford-Cars	55.7	2.3	51.7	64.5	65.4	**66.3**
STL10	**98.0**	97.4	96.9	97.7	97.5	97.6
SUN397	**47.1**	6.9	25.6	0.2	0.2	0.2
cub	46.0	3.3	45.5	72.2	63.3	**75.6**
ImageNet	**60.2**	0.8	57.7	56.8	53.6	59.8
ImageNet-r	**68.9**	1.7	63.3	54.9	47.6	57.1
ImageNet-Sketch	39.8	0.8	40.4	43.4	37.9	**48.3**
Amazon	74.0	47.9	**89.1**	71.3	66.9	71.3
CivilComments	48.3	**69.1**	55.8	53.8	45.5	53.8
Gender	84.0	57.0	**87.8**	78.0	71.2	78.5
HateXplain	30.4	34.4	**35.2**	32.8	32.7	32.3

Table 12. Accuracy (%) with OTTER combined with class balance estimation. ZS BBSE denotes BBSE class balance estimation based on zero-shot prediction scores, and LP BBSE denotes BBSE class balance estimation based on linear probing prediction scores. We report the mean of 10 different random samplings of the validation set.

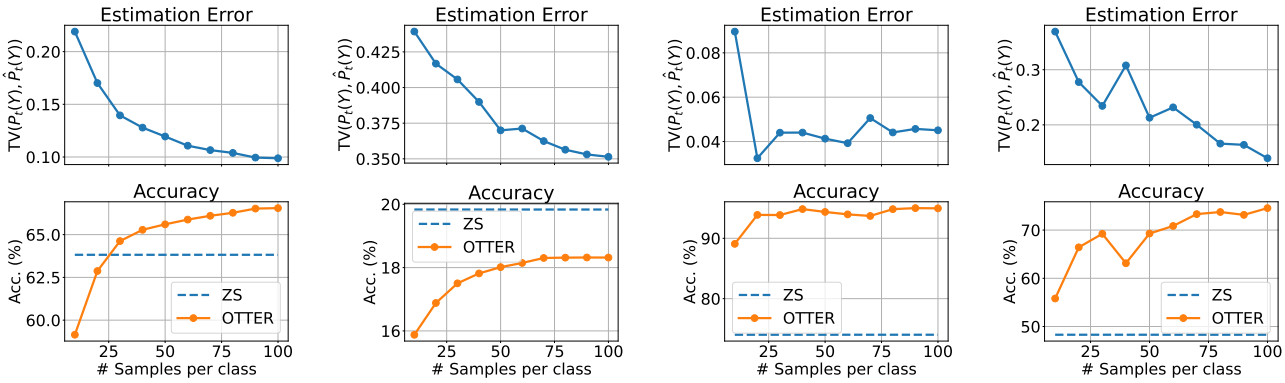

(a) CIFAR100 (b) Country211 (c) Amazon (d) CivilComments

Figure 4. Ablation experiment on the number of samples. We report the mean of 10 different samplings in each setting. We use ViT-B/16 for image classification, and BERT for text classification.

E.6. Zero-shot prediction improvement with class hierarchy

We hypothesize incorporating class hierarchy information can enhance few-shot label distribution estimation and thus improve zero-shot predictions.

Setup and Procedure. We use a subset of CIFAR100 data with WordNet hierarchy. Specifically, we take 'fish' and 'tree' as superclasses and have 5 subclasses in each of them. We suppose we can access 10 labeled samples per each subclass. We first apply OTTER with the superlevel label distribution estimation and make pseudo-labels of superlevel class in the test set. Using them, we estimate the sublevel label distribution and use OTTER.

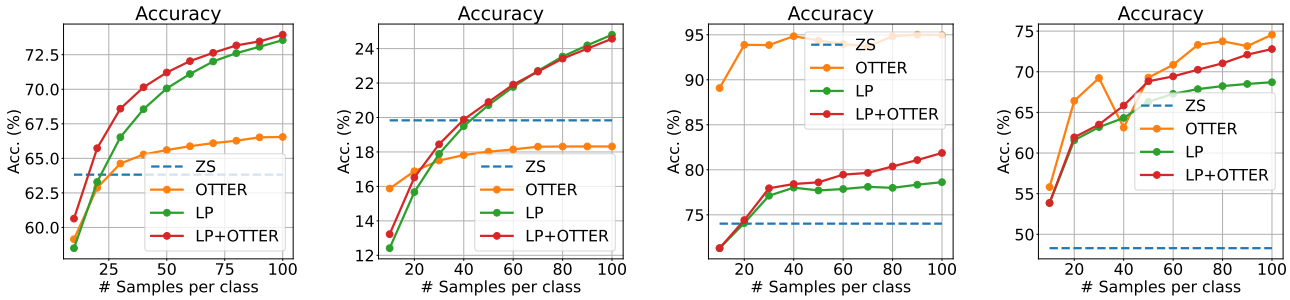

(a) CIFAR100 (b) Country211 (c) Amazon (d) CivilComments

Figure 5. Comparison between OTTER, LP, and LP+OTTER with varying the number of samples. We report the mean of 10 different samplings in each setting. We use ViT-B/16 for image classification, and BERT for text classification.

Results. Table 13 presents the results. As anticipated, we note an enhancement in accuracy when compared to the naive implementation of OTTER. Specifically, we observe a significant improvement in accuracy for RN50, RN101, and ViT-B/16, which we attribute primarily to the reduction in label distribution estimation error. Further details are provided in Appendix E.7.

	OTTER	H-OTTER
RN50	38.5 (±4.9)	**43.6** (±3.1)
RN101	39.9 (±6.9)	**44.8** (±5.1)
ViT-B/32	59.0 (±3.1)	**59.3** (±2.9)
ViT-B/16	54.6 (±8.3)	**58.2** (±3.6)
ViT-L/14	**71.3** (±3.9)	69.4 (±5.2)

Table 13. Accuracy (%) with hierarchical OTTER (H-OTTER). We report the mean and the standard deviation of 10 different random samplings of the labeled data.

E.7. Detailed experiment setup and results of Section E.6

Class hierarchy We used the following superclasses and subclasses classes for the proof of concept.

- fish: aquarium fish, flatfish, ray, shark , trout
- tree: maple tree, oak tree, palm tree, pine tree, willow tree

Class balance estimation error We report the class balance estimation error in Section E.6. Table 14 shows the total variation between true class balance and estimated class balance. We can expect a significant accuracy improvement for RN50, RN101, and ViT-B/16 based on this table.

	BBSE	H-BBSE
RN50	0.335	**0.246**
RN101	0.378	**0.294**
ViT-B/32	**0.156**	0.167
ViT-B/16	0.287	**0.246**
ViT-L/14	**0.131**	0.152

Table 14. Class balance estimation error in the Section E.6 experiment. Class balance estimation error is measured by total variation distance. We report the mean of 10 different samplings of the validation set. H-BBSE denotes the class balance estimation using hierarchy upon BBSE.